Linkage Disequilibrium with Linkage Analysis of Multiline Crosses Reveals Different Multiallelic QTL for Hybrid Performance in the Flint and Dent Heterotic Groups of Maize

Héloïse Giraud,* Christina Lehermeier,† Eva Bauer,† Matthieu Falque,‡ Vincent Segura,§ Cyril Bauland,‡ Christian Camisan, Laura Campo,†† Nina Meyer,‡‡ Nicolas Ranc,§§ Wolfgang Schipprack,*** Pascal Flament,** Albrecht E. Melchinger,*** Monica Menz,§§ Jesús Moreno-González,†† Milena Ouzunova,‡‡ Alain Charcosset,‡ Chris-Carolin Schön,† and Laurence Moreau‡,1**

*Université Paris-Sud, Unité Mixte de Recherche 0320/Unité Mixte de Recherche 8120 Génétique Végétale, F-91190 Gif-sur-Yvette, France, †Plant Breeding, Technische Universität München, D-85354 Freising, Germany, ‡Institut National de la Recherche Agronomique, Unité Mixte de Recherche 0320/Unité Mixte de Recherche 8120 Génétique Végétale, F-91190 Gif-sur-Yvette, France, §Institut National de la Recherche Agronomique, F-45075 Orléans, France, **Limagrain Europe, F-63720 Chappes, France, ††Centro Investigacións Agrarias Mabegondo, 15080 La Coruña, Spain, ‡‡Kleinwanzlebener Saatzucht Saat AG, D-37555 Einbeck, Germany, §§Syngenta Seeds, F-31790 Saint-Sauveur, France, and ***Institute of Plant Breeding, Seed Science and Population Genetics, University of Hohenheim, D-70593 Stuttgart, Germany

ABSTRACT Multiparental designs combined with dense genotyping of parents have been proposed as a way to increase the diversity and resolution of quantitative trait loci (QTL) mapping studies, using methods combining linkage disequilibrium information with linkage analysis (LDLA). Two new nested association mapping designs adapted to European conditions were derived from the complementary dent and flint heterotic groups of maize (*Zea mays* L.). Ten biparental dent families ($N = 841$) and 11 biparental flint families ($N = 811$) were genotyped with 56,110 single nucleotide polymorphism markers and evaluated as test crosses with the central line of the reciprocal design for biomass yield, plant height, and precocity. Alleles at candidate QTL were defined as (i) parental alleles, (ii) haplotypic identity by descent, and (iii) single-marker groupings. Between five and 16 QTL were detected depending on the model, trait, and genetic group considered. In the flint design, a major QTL ($R^2 = 27\%$) with pleiotropic effects was detected on chromosome 10, whereas other QTL displayed milder effects ($R^2 < 10\%$). On average, the LDLA models detected more QTL but generally explained lower percentages of variance, consistent with the fact that most QTL display complex allelic series. Only 15% of the QTL were common to the two designs. A joint analysis of the two designs detected between 15 and 21 QTL for the five traits. Of these, between 27 for silking date and 41% for tasseling date were significant in both groups. Favorable allelic effects detected in both groups open perspectives for improving biomass production.

MOST traits of agronomic interest present a continuous variation resulting from the sum of the effects of various quantitative trait loci (QTL). Mapping these QTL is a first step toward elucidating their molecular nature and offers important application perspectives for marker-assisted breeding. QTL mapping started in plants with segregating families derived from the cross of two inbred lines (Lander and Botstein 1989). However, such biparental designs address only a small portion of the diversity available (a maximum of two alleles can segregate at a given QTL) and the accuracy of QTL positions is usually poor. To overcome these limitations, Rebai and Goffinet (1993) and Charcosset *et al.* (1994) proposed models for joint QTL detection in several biparental families connected to each other by the use of common parental lines. When the number of parents is less than the number of families, connections can be taken into

doi: 10.1534/genetics.114.169367
Manuscript received August 6, 2014; accepted for publication September 23, 2014; published Early Online September 29, 2014.
Supporting information is available online at http://www.genetics.org/lookup/suppl/doi:10.1534/genetics.114.169367/-/DC1.
[1]Corresponding author: Institut National de la Recherche Agronomique, Unité Mixte de Recherche 0320/Unité Mixte de Recherche 8120 Génétique Végétale, F-91190, Gif-sur-Yvette, France. E-mail: moreau@moulon.inra.fr

account to reduce the number of allelic effects to be estimated in the detection model. This increases power and accuracy of detection when QTL behave additively (see Blanc *et al.* 2006). However, such a model makes the assumption that each parental line carries a different allele, which limits its benefit when the number of parental lines is high relative to the number of families, a situation commonly encountered in breeding programs.

Recent advances in sequencing and genotyping technologies make it possible to genotype individuals for a large number of markers at reduced costs, so that one can expect to have markers closely linked to any QTL. This has paved the way toward association mapping, in which marker-trait associations are directly detected in populations composed of diverse inbred lines without the need to develop experimental segregating families. Association mapping, also often referred to as linkage disequilibrium (LD) mapping, has been widely used with success in the plant community (see for instance Bouchet *et al.* 2013 and Romay *et al.* 2013 for recent results of association mapping in maize). In this approach, it is important to use models accounting for potential underlying population structure and relatedness between individuals to prevent spurious QTL detection due to associations between loci that are not linked physically (Yu *et al.* 2006). As a consequence, the power to detect associations is low for causal polymorphisms correlated with the underlying population structure or when they are present in the population at a low frequency (Rincent *et al.* 2014). In addition, associations are generally tested at SNP (single nucleotide polymorphism) markers, which leads to the implicit assumption that the QTL are biallelic. These limitations can be alleviated by combining information coming from LD at the level of the parents and linkage within families, as first proposed for animal populations by Meuwissen and Goddard (2001). In this approach, referred to as linkage disequilibrium and linkage analysis (LDLA), dense genotyping of parents is used to detect identity by descent (IBD) at putative QTL, *i.e.*, the fact that two individuals carry the same allele transmitted by a common ancestor. Different types of LDLA analyses have been proposed to account for the LD component. The simplest is to consider that parents carrying the same allele at a given marker are IBD (Yu *et al.* 2008; Liu *et al.* 2012) as done in association mapping. Haplotype-based approaches also have been proposed to group parental alleles and tested by simulations (for instance Jansen *et al.* 2003; Bink *et al.* 2012; Leroux *et al.* 2014). Advantages of LDLA have been shown experimentally in maize notably by using the nested association mapping (NAM) design developed in the United States (Yu *et al.* 2008; McMullen *et al.* 2009). This design consists of 25 biparental recombinant inbred line (RIL) populations derived from the cross of the inbred B73 with 25 diverse lines representing the diversity of maize (tropical, temperate, sweet corn, and popcorn lines). This design was studied with a linkage analysis model (Buckler *et al.* 2009; Kump *et al.* 2011; Tian *et al.* 2011) where QTL effects were nested within each family and each parental line was assumed to carry a different allele, and with LDLA through a genome-wide association mapping model (Kump *et al.* 2011; Tian *et al.* 2011) including allelic effects observed at individual SNP of the parents to identify IBD alleles. This design successfully led to the detection of numerous QTL and use of LDLA permitted in some cases to resolve QTL detection up to the gene level (Kump *et al.* 2011; Poland *et al.* 2011; Tian *et al.* 2011; Cook *et al.* 2012). Recently, Bardol *et al.* (2013) applied the haplotype-based approach of Leroux *et al.* (2014) to detect QTL in two data sets coming from an applied maize (*Zea mays* L.) breeding program and compared it to models considering each parental allele as different (linkage model) or considering that parents carrying the same allele at a given marker are IBD. Results showed that when parental lines are all issued from the same breeding program and related by pedigree, LDLA models were more powerful than linkage approaches. Bardol *et al.* (2013) also showed that the different ways of modeling allelic variation (either using haplotypes or single-marker information) had variable efficiencies depending on the QTL and trait considered and were therefore complementary. It is thus important to further evaluate the ability of diverse LDLA models to detect QTL in multiparental populations with different diversity levels.

The central line of the U.S. NAM (B73) is too late flowering for evaluation in Northern Europe and founder lines cover a very broad range of geographical origins, including even later tropical materials. This prevents the evaluation of the whole design for productivity traits in Northern European conditions and due to diversity of the lines it is difficult to use a single tester to investigate hybrid values. To overcome these limitations and expand the genetic pool investigated in maize QTL mapping studies, two parallel complementary NAM designs were developed within the European project CornFed. Each was derived from inbred lines representing the main diversity available for breeding in each of the two major heterotic groups (dent and flint) used in Northern Europe. Both designs were genotyped with a 50k SNP array (Ganal *et al.* 2011) and genotyping information was used to build individual population maps (Bauer *et al.* 2013). The two NAM designs were crossed with the central line of the opposite group to produce hybrids, which were analyzed for traits related to biomass production as described in Lehermeier *et al.* (2014). Increasing biomass production is of key interest in Northern Europe where maize has been extensively used for decades for silage and more recently for bioenergy production. To our knowledge no QTL mapping experiment has been carried out so far for traits related to biomass production in multiparental design assembling such large diversity. Note that both hybrid designs address variation compared to the same hypothetical reference hybrid (the one produced by crossing the two central lines), with each experimental hybrid of each group sharing on average 75% of its genome with the reference hybrid. In this context, effects of all

segregating genotypes at a QTL (11 on the dent side and 12 on the flint side) are compared to a same genotype (having received alleles from two central lines). This makes this design particularly adapted for deciphering loci involved in genetic variation on the dent and flint sides for productivity traits.

This study aimed at comparing different methods of QTL detection in these two European NAM designs for five traits of agronomical interest for biomass production in maize: whole plant dry matter yield, whole plant dry matter content at harvest, female flowering, male flowering, and plant height. We compared a linkage approach with two LDLA approaches either considering haplotypic IBD or single-marker groupings. This allowed us to investigate the performance of the different LDLA approaches in two complementary heterotic groups in a more diverse context than a simple breeding program. A second important objective of this work was to compare the results of QTL detection conducted separately in the two heterotic groups or jointly for the whole design, to better understand the contribution of each group to trait variation.

Material and Methods

Plant material and phenotypic analysis

Two maize NAM designs composed of half-sib families from the two major heterotic groups (dent and flint) used for breeding in Europe were analyzed. The two designs are described in Bauer *et al.* (2013). In short, the dent and flint designs were respectively composed of 10 and 11 doubled haploid (DH) families, derived from the cross of respectively 10 and 11 diverse founder lines with a common central line: F353 for the dent and UH007 for the flint. F353 and UH007 represent very promising European lines created by public institutes in their respective heterotic groups. The parental lines were chosen to cover the diversity available within the two groups with a combination of ancestral and more recent material. From each cross, DH lines were generated, resulting in 919 lines for the dent and 1009 for the flint (Bauer *et al.* 2013) (Supporting Information, Table S1). For phenotypic evaluation (see below), the segregating DH lines of a given group were crossed with the central line of the other group. A total of 841 hybrids were produced for the dent group and 811 for the flint group (Lehermeier *et al.* 2014) (Table S1). The number of dent lines for which testcrossed progenies were phenotyped per family was 84 on average and varied between 53 and 104, depending on the family. For the flint group, the number of DH lines per family that were phenotyped for testcross values ranged from 17 to 133 with an average of 73. As the hybrids of each group were obtained by crossing DH lines with the central line of the other group, all the hybrids shared a large proportion of their genome and were expected to be heterozygotes F353/UH007 for 50% of their genome. Hybrids were evaluated in 2011 in four (dent) and six (flint) European locations. Five traits were considered: biomass dry matter yield (DMY, decitons per hectare, $dt \cdot ha^{-1}$) at the whole plant level, whole plant dry matter content (DMC, %) at harvest, days to tasseling (DtTAS, in days), and days to silking (DtSILK, in days) measured as the number of days from sowing until tasseling and silking, respectively. Field trial design is described in Lehermeier *et al.* (2014). Individual field plot measures were analyzed (Lehermeier *et al.* 2014) to compute for each hybrid the adjusted means over the different trials that were used in this study.

Genotyping and analysis of genotypic data

The 1928 DH lines and the 23 parental lines were genotyped with the Illumina MaizeSNP50 BeadChip containing 56,110 SNPs (Ganal *et al.* 2011). Markers with a call frequency <0.9, a GenTrainScore <0.7, a minor allele frequency (MAF) <0.01, or $>10\%$ missing values were discarded as in Lehermeier *et al.* (2014).

Consensus maps for the flint and the dent multipopulations were obtained following the same procedure. We considered for each consensus map the list of markers present in at least 1 of the 10 dent individual maps (respectively, 11 flint individual maps) from Bauer *et al.* (2013). The flint DH family resulting from the cross of EP44 and UH007 was not used due to small population size. For each marker of this list and for each individual genetic map, we computed the relative genetic position of this marker in this map by starting from its physical coordinate on the B73 genome assembly and converting it into a genetic coordinate with the spline-smoothing interpolating procedure described in Bauer *et al.* (2013). These genetic coordinates were then normalized between zero and one to obtain relative genetic positions. For the present study, each consensus map was built by computing the consensus relative genetic position of each marker as the average of its relative genetic positions in all individual maps involved, weighted by the numbers of individuals in the corresponding populations. Finally, the consensus genetic coordinate of each marker was obtained by multiplying its consensus relative genetic position by the genetic length of the consensus map, taken as the average of the genetic lengths of all maps, weighted by the numbers of individuals in the corresponding populations. The two consensus maps obtained are available at Maize GDB (http://maizegdb.org/cgi-bin/displayrefrecord.cgi?id=9024747, data available on 4th November 2014). A consensus map for the dent and flint multipopulations was built with the same procedure.

For the QTL detection we considered in the analysis only the PANZEA markers which were mapped on the consensus maps. PANZEA markers result from the alignment of sequences coming from resequencing data of the 27 lines used as parents of the U.S. NAM design (McMullen *et al.* 2009) and mapped against the B73 genome v. 2 (Gore *et al.* 2009). We discarded the other markers, mainly defined by comparing the sequences of the inbred lines B73 and Mo17, as they are known to create an ascertainment bias in diversity

Table 1 Number of mapped markers, length of the genetic map and linkage disequilibrium decay modeled with the Hill and Weir (1988) model for a r^2 = 0.2 for the two groups dent and flint for each chromosome and for the whole genome

	Dent			Flint		
Chromosome	Markers	Length (cM)	LD decay (cM)	Markers	Length (cM)	LD decay (cM)
1	3287	184.5	0.96	2892	237.2	0.76
2	2402	137.9	2.51	2264	182.7	0.65
3	2480	151.0	1.99	2410	156.4	0.45
4	2528	134.6	1.47	2379	165.5	0.65
5	2405	136.6	0.45	2322	180.6	0.35
6	1695	119.9	1.47	1544	134.9	0.65
7	1820	128.9	1.37	1709	149.7	0.76
8	1992	125.6	1.47	1756	139.7	0.45
9	1699	118.5	0.96	1610	133.5	0.76
10	1570	105.8	1.89	1520	106.1	0.76
Genome	21878	1343.3	1.2	20406	1586.3	0.65

analyses (Ganal *et al.* 2011; Frascaroli *et al.* 2013).The dent and flint consensus genetics maps obtained were composed of, respectively, 21,878 and 20,406 PANZEA markers, corresponding respectively to 6808 and 7272 genetic positions on the consensus maps. The dent-flint consensus map was composed of 25,472 PANZEA markers, corresponding to 8124 genetic positions (Table 1).

Clustering analysis of parental inbred lines

Clustering of the parental inbred lines was carried out with the R package "clusthaplo" (Leroux *et al.* 2014), separately on the dent and flint parents. This clustering was based on genomic similarities computed between each pair of individuals in a sliding window along the genome. To obtain insight into the length of the sliding window to use, we evaluated how fast LD between pairs of markers decays with the genetic distance. LD between pairs of markers was estimated for the 11 dent founder lines and for the 12 flint founder lines, according to Hill and Robertson (1968) as $r^2 = D_{AB}^2/(p_A(1-p_A)p_B(1-p_B))$, with $D_{AB} = p_{AB} - p_A p_B$, where p_{AB} denotes the haplotype frequency of AB, p_A the frequency of allele A at one marker locus, and p_B the frequency of allele B at the other locus. The LD decay was estimated using the Hill and Weir (1988) model. The choice of the sliding window size was based on the LD decay observed in the dent and flint material considering the length in genetic distance needed to reach an $r^2 < 0.2$. Two values were chosen, 2 and 5 cM, each based on the LD decay observed for the flint and dent group, respectively. For facilitating comparisons between results obtained in the two groups, the clustering was carried out in each group using the two window sizes.

For each window size at each genotyped position, the similarity score between two parental lines i and j at a position t (center of the window) was calculated according to the formula described in Leroux *et al.* (2014) and used in Bardol *et al.* (2013). This formula is adapted from Li and Jiang (2005) and combined the number of alleles alike-in-state between the two lines inside the sliding window and the length of their longest common segment centered on t. Based on the similarity score curves obtained along each chromosome, a hidden Markov model (HMM) was used to determine at each position t if the two lines were similar and thus carried the same ancestral allele or not. After the clustering process, the number of ancestral alleles per position was plotted along chromosomes. We also computed similarities between inbred lines as the percentage of ancestral alleles shared over the genome and compared them with the similarities obtained from the SNP markers. A graphical representation of these similarities and a classification of the parental lines were carried out using the "heatmap" function in R (R Core Team 2013).

QTL detection

Analyses were first performed separately for each trait on the dent and flint multifamily designs, using their respective consensus map. Four statistical models were tested: one based on linkage analysis and three others combining linkage and LD information. All the models were multilocus models in which the significance of each QTL was tested, conditional on the inclusion of other QTL positions used as cofactors.

The first model corresponded to a conventional multifamily connected model. This model considered the connections between families through the sharing of the central inbred line and relied on the assumptions that each parental inbred line carried a different QTL allele and that each allelic effect was independent of the family

$$y = J.\mu + X_{\mathrm{q}}.a_{\mathrm{q}} + \sum_{\mathrm{c}\neq\mathrm{q}} X_{\mathrm{c}}.a_{\mathrm{c}} + e,$$

where y was the vector ($N \times 1$) of the adjusted phenotypic means of the N individuals of the data set, J was a ($N \times P$) matrix of 0 and 1 that linked each individual to the family it belonged to with P being the total number of families, μ was the column vector ($P \times 1$) of family means, and X_{q} and X_{c} were ($N \times K$) matrices with K being the number of parents. Each element (ranging from 0 to 2) of these matrices corresponded to the expected number of alleles of the parent k at

QTL q and cofactor c for each individual, according to the genotyping information at the position of q and c when this information was available (*i.e.*, when these positions correspond to markers polymorphic in the population the individual belong to) or at flanking markers otherwise. a_q and a_c were the column vectors ($K \times 1$) of the additive intrafamily effects associated with QTL q and cofactor c, respectively. e was a column vector ($N \times 1$) of the residuals of the model. This model will be further referred to as "connected." Note that this model is close to the joint inclusive composite interval mapping (JCIM) model proposed by Buckler *et al.* (2009) and used on the U.S. NAM design.

The second and third models were LDLA multifamily connected models, which used the results of the clustering of parental alleles carried out with clusthaplo

$$y = J.\mu + X_q.Q_q.h_q + \sum_{c \neq q} X_c.Q_c.h_c + e,$$

where y, J, μ, X_q, X_c, and e were the same as described as in the previous model. Q_q and Q_c were ($K \times A_q$) and ($K \times A_c$) matrices with A_q and A_c being the number of ancestral alleles at QTL q and cofactor c. Each element (0 or 1) of these matrices linked the parental alleles at QTL q and cofactor c to the ancestral alleles identified by the clustering approach. h_q and h_c were column vectors ($A_q \times 1$) and ($A_c \times 1$) of the additive effects of the ancestral alleles associated with QTL q and cofactor c. Two models were considered, one based on the clustering approach using a window size of 2 cM and further referred to as "LDLA—2 cM," and one based on the clustering approach using a window size of 5 cM and further referred to as "LDLA—5 cM."

QTL detection using the three models described above were performed using the MCQTL_LD software (Jourjon *et al.* 2005) using an iterative composite interval QTL mapping method (iQTLm) (Charcosset *et al.* 2000). For these models, genotypic information of markers located at the same position of the consensus genetic map was concatenated to indicate which parental allele was transmitted. For missing data, MCQTL_LD software estimated the probability of transmission of each parental allele based on the information of flanking markers. At each tested position, the presence of a QTL was assessed based on the $-\log10$ of the Fisher test P-value [$-\log10(P\text{-value})$]. Thresholds for considering a QTL as significant were computed for each trait and each data set using 5000 intrafamily permutations of the phenotypes for a type I risk of 10% across all families and total genome. In the iQTLm approach, the initial set of cofactors was chosen using a multiple regression with a forward selection of marker positions with a threshold equal to 80% of the QTL significance threshold value. At the end of the detection process, for the conventional connected model, confidence intervals at 95% were estimated on the basis of a 1 LOD unit fall. The confidence intervals were not estimated for the LDLA models as there is no established method proposed for these models.

The fourth model, referred to as single-marker LDLA model ("LDLA—1-marker"), considered that two parental lines carrying the same allele at a marker were IBD for this marker

$$y = J.\mu + M_q.g_q + \sum_{c \neq q} M_c.g_c + e.$$

y, J, μ, and e were as described in the previous model. M_q and M_c were ($N \times 2$) matrices whose elements (0 or 1) corresponded to the genotyping information at QTL q and cofactor c for each individual. g_q and g_c were column vectors (2×1) of the additive effects of marker alleles associated with QTL q and cofactor c. This model can be viewed as a multilocus genome-wide association study with population structure controlled by family membership. It is equivalent to the association mapping model used to analyze the U.S. NAM design (Yu *et al.* 2008; Tian *et al.* 2011; Kump *et al.* 2011) except that in our model, dense marker genotyping information is directly available for the progenies and does not need to be inferred from the parental genotypes.

The analysis with the fourth model was performed in R (R Core Team 2013) using an R-script derived from the one used for the multilocus mixed model approach presented in Segura *et al.* (2012). We used a multilocus forward–backward stepwise linear regression model and selected the most appropriate model using the extended Bayesian information criterion (Segura *et al.* 2012). Loci of the selected model, which had P-values below the Bonferroni threshold for a genome-wide risk of 10%, were considered as QTL. For this model, imputation of the genotyping data for marker with missing data were done using the software BEAGLE (Browning and Browning 2009) family by family. Even if we considered the same type I error risk at the genome level as for other models, the threshold used for the LDLA—1-marker model was not obtained by permutations and is possibly more conservative than other models.

Analyses were then performed jointly for each trait on the two designs using the dent–flint consensus map. The model used corresponded to a conventional multifamily connected model except that all the dent and flint families were considered jointly. As the central line of the dent is used as tester in the flint design and reciprocally, the F353-UH007 genotype segregates against an alternative genotype in each population. This enabled us to connect allelic effects estimated in the two designs. QTL detection was performed using the MCQTL_LD software (Jourjon *et al.* 2005) following the same procedure as that used in group-specific QTL detection. Thresholds for considering a QTL as significant were computed for the joint data set for each trait using 5000 intrafamily permutations of the phenotypes for a type I risk of 10% across all families and total genome. To test whether effects were significant in a single group or in both groups, the effects of the QTL detected in the joint analysis were tested in each of the separate data sets. They were considered as significant if the $-\log10$ of the Fisher test

P-value was above the thresholds of the studied trait in the separate data set (estimated with the dent or flint consensus maps, respectively).

For each analysis, variances explained by each QTL (partial R^2_{QTL}) were defined as the ratio between the sum of squares associated with the QTL effect in the model including the other detected QTL and the residual sums of squares of a linear model considering only the family effects. Total percentage of variance explained by the detected QTL (R^2_{total}) was defined as the ratio between the sum of squares of all the detected QTL and the residual sums of squares of a linear model considering only the effects of the families. All the R^2 were adjusted by the number of degrees of freedom of the considered models (Charcosset and Gallais 1996). Differences in effects among pairs of alleles at a given QTL were tested *a posteriori* using a *t*-test ($\alpha = 5\%$). For facilitating comparisons between models and the interpretation of the QTL results, the allelic effect of the central lines were set to zero, and the other allelic effects were estimated accordingly.

Comparison of the positions of the QTL detected separately in the two groups and in the joint analysis was based on the results of the connected model. QTL detected in each separate group and on the joint data set were projected on the dent–flint consensus map using BioMercator v. 4.2 (Sosnowski *et al.* 2012). A QTL was considered common for a trait when the confidence intervals of the QTL after projection were overlapping.

Results

Analysis of parental linkage disequilibrium and parental clustering

The average genetic distance to reach a LD below $r^2 = 0.2$ was 1.2 and 0.65 cM for the dent and flint groups, respectively (Table 1). This distance varied according to the chromosome between 0.45 cM (chromosome 5) and 2.51 cM (chromosome 2) for the dent group and 0.35 cM (chromosome 5) and 0.76 cM (chromosomes 1, 7, 9, 10) for the flint group. The two different sliding window sizes that we considered for computing the similarity score with clusthaplo approximately correspond to two times the distance beyond which LD becomes negligible for all the chromosomes. Note that 2 cM was the minimum window size that we could consider since the HMM-based clustering approach did not converge for smaller window sizes.

The 5-cM sliding window size led to a higher number of ancestral alleles than the 2 cM one for the two designs. For dent, the average number of ancestral alleles along the genome was 5.6 per genetic position for the 2-cM sliding window size and 6.5 for the 5-cM window. For flint, the average number of ancestral alleles was 5.9 per genetic position for the 2-cM sliding window size and 7.2 for the 5-cM window. It has to be noted that the number of ancestral alleles varied along the genome. For both window sizes, clustering was more important in telomeric than in centromeric regions, where quite often the number of ancestral alleles equaled the number of parental lines (Figure 1).

For both sliding window sizes, similarities between the parental inbred lines estimated based on ancestral alleles sharing showed a structured pattern (Figure 2). Within the dent group, pairs of lines involving (i) UH250, D09, and D06 and (ii) F353 and UH304 shared the same ancestral alleles for >47% of the genetic positions for both sizes of sliding window. In the flint group, with the 5-cM window, closest pairs of lines involved UH006, UH007, and UH009. With the 2-cM window size, this expanded to F03802, D152, and F2. The classifications of parental lines based on single markers were globally consistent with those based on ancestral alleles, at least for grouping the most similar lines. Only positions of inbred lines that showed low levels of similarities with the other lines slightly changed in the dendrogram depending on the allele definition considered. In the dent group, three related lines, UH250, D09, and D06, are clearly separated from a nonstructured group among which only F353 (the central line of the dent design) and UH304 were related. In the flint group, similarities separated a subgroup composed of F64, EC49A, EZ5, and EP44 from the other lines that appeared to be more closely related to each other. In this subgroup, UH009 and UH006 are both related to UH007, the central line of the flint design.

Comparison of the thresholds used in the QTL detection models

For the separate data sets analyses, threshold values [−log10(*P*-value)] were higher for the LDLA models than for the linkage model (Table S2). For LDLA models, the threshold increased as the size of the considered window decreased. This suggests that reducing the size of the window decreases the dependence between tests. For every model, threshold values were lower for DMC and higher for DtSILK and DtTAS (except for the conventional connected model for the flint group). This might be due to heterogeneity of within-family variances for some traits. For instance, for DtSILK, for the dent data set, genetic variances varied from 0.95 to 4.93 (see Lehermeier *et al.* 2014 for an estimation of these variances). As for the separate data sets thresholds, for the joint data set, threshold values for the connected model were lower for DMC and higher for DtSILK and DtTAS.

Comparison of the QTL detected with the different models in the dent and flint designs

For a given trait and group, the number of detected QTL varied according to the model (Table 2, Table S3, Table S4, Table S5, Table S6, Table S7, Table S8, Table S9, and Table S10). Between 5 (for DMY with LDLA—5 cM and LDLA—1-marker models) and 16 (for DMC with LDLA—2 cM model) QTL were detected in the dent design and between 7 (for DMC with LDLA—1-marker model) and 16 QTL (for DtSILK and DtTAS with LDLA—1-marker model) in the flint design.

For the dent group, the LDLA—1-marker model detected fewer QTL over all traits (45 QTL in total) and explained the

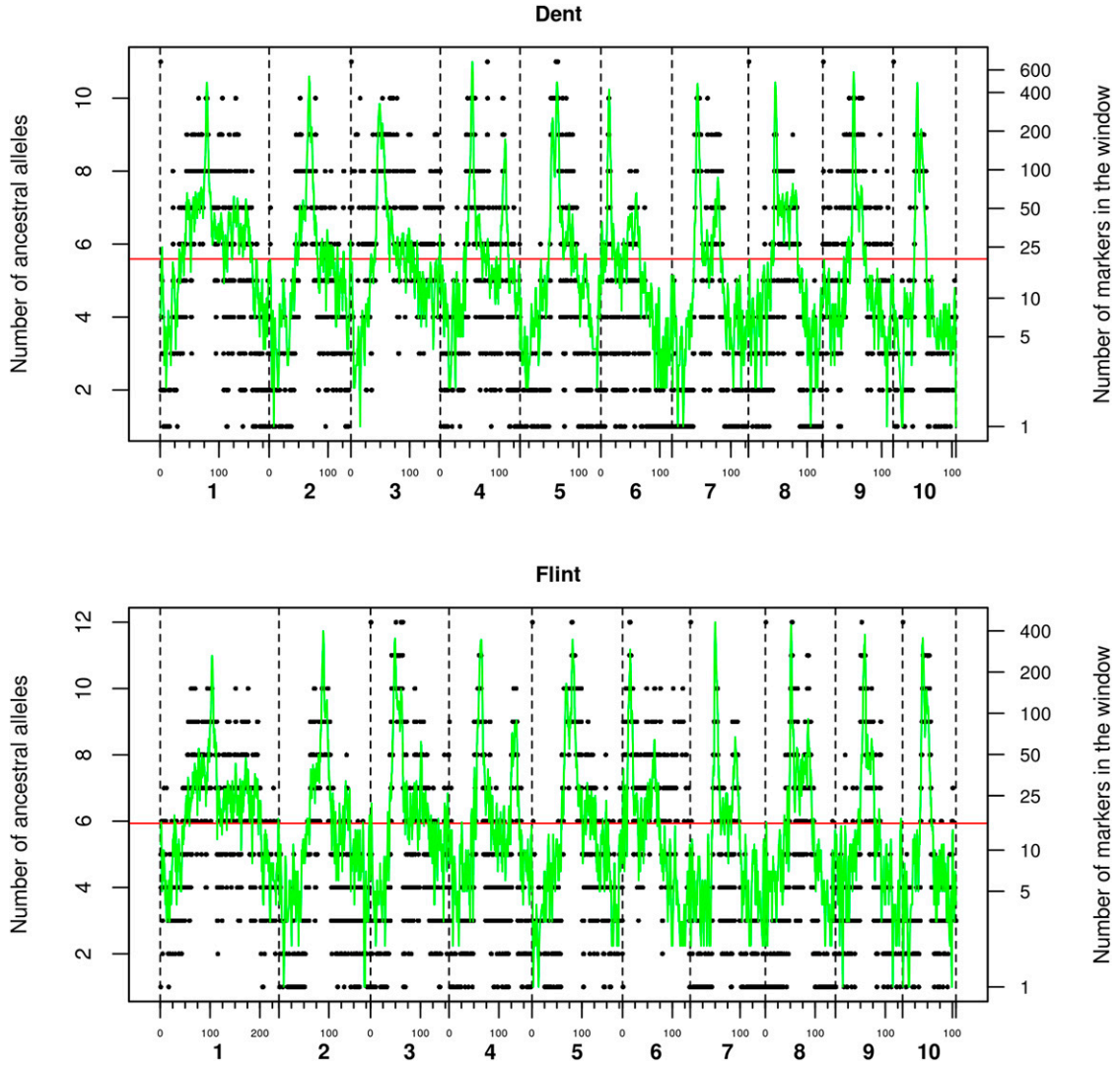

Figure 1 Number of ancestral alleles along the genome after clustering with clusthaplo using a 2-cM sliding window size and number of markers in the 2-cM sliding window along the genome for the dent design (6808 unique positions on the genome—1343.3 cM in total) and the flint design (7272 unique positions on the genome—1586.3 cM in total). The black points correspond to the number of ancestral alleles. The green line corresponds to the number of markers in the 2-cM sliding window along the genome. Horizontal red lines correspond to the average number of ancestral alleles along the whole genome. The vertical black dotted lines correspond to the limits of each chromosome.

smaller percentage of variance (33.8% on average). In this group, the LDLA models using clusthaplo information detected more QTL (56 in total for the LDLA—5 cM, 55 for the LDLA—2 cM) than the conventional connected model (52 QTL in total). This advantage of the LDLA models in terms of number of QTL detected was found for DMC, DtSILK, and DtTAS. In contrast, for DMY and PH the connected model detected more QTL. Even if more QTL were detected on average with the LDLA models, the connected model explained a higher percentage of variance (46.9%) than the other models.

For the flint group, the LDLA—1-marker model detected more QTL (59 QTL in total) but explained a smaller percentage of variance (47.3% on average) than the other models. In this group, the conventional connected model detected the smallest number of QTL (55 in total). The LDLA models using clusthaplo information detected an intermediate number of QTL (58 and 56 for the LDLA—5 cM and LDLA—2 cM models, respectively). The ranking of the models in terms of number of detected QTL varied depending on the trait. For instance, the two LDLA models using clusthaplo information detected more QTL than the conventional connected model for DtTAS, PH, DMC (with the LDLA—5 cM model only), and for DMY (with the LDLA—2 cM model only). For the flowering traits, the LDLA—1-marker model detected more QTL than the other models. As for the dent group, the connected model explained a higher percentage of variance (56.3%) compared to the other models even if it did not detect a higher number of QTL.

One can note that the $-\log10(P\text{-values})$ curves showed relatively noisy patterns along the genome, especially for the LDLA models (Figure 3, Figure S1, Figure S2, Figure S3, and

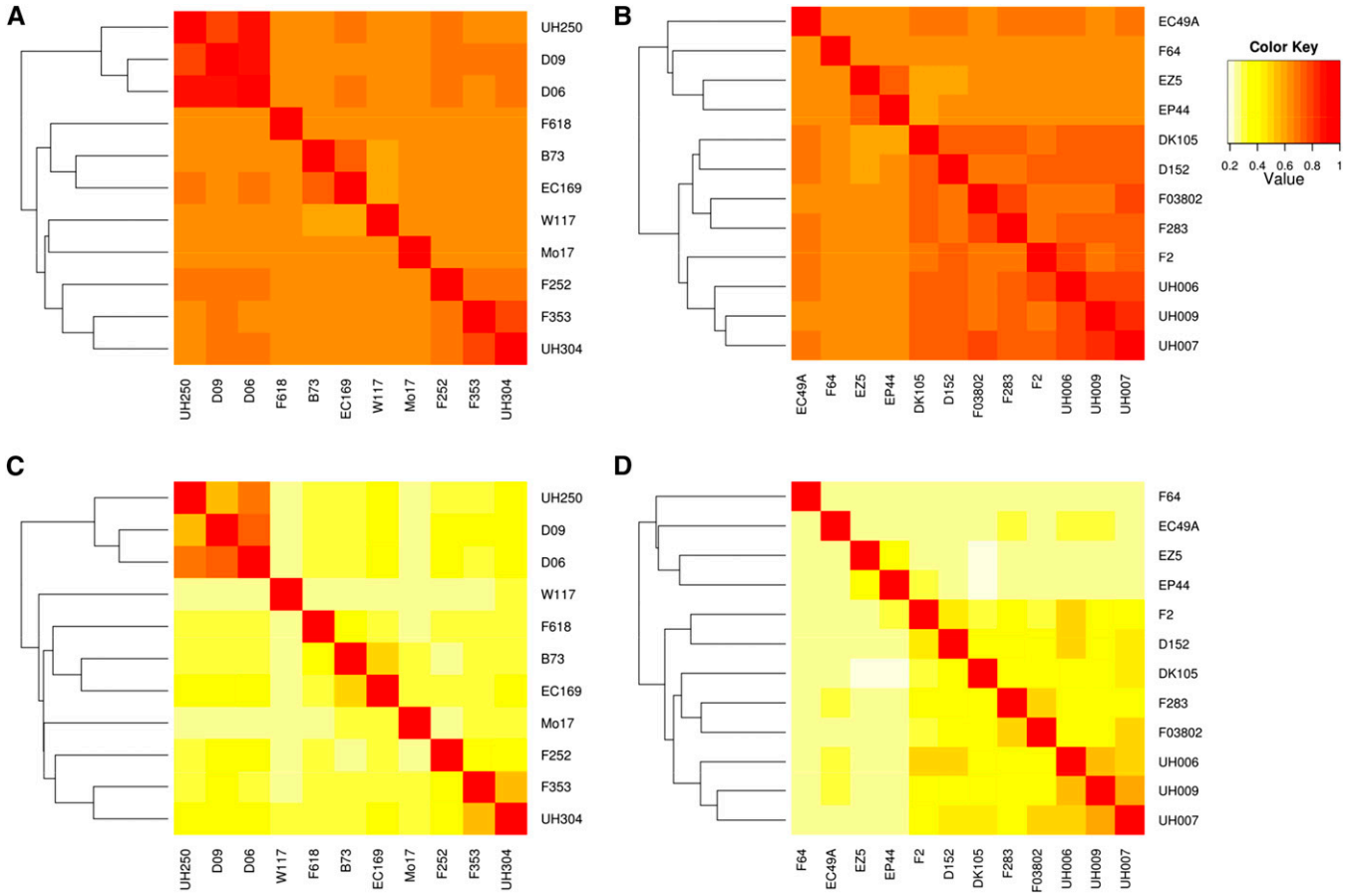

Figure 2 Similarities between the dent (left) and the flint parental lines (right), computed based on direct marker genotyping (top) and on ancestral allele sharing (using clusthaplo and a 2-cM window size) (bottom). Yellow corresponds to a low similarity, red corresponds to a high similarity (color scale on the top-right corner). Lines were ordered according to their position in the dendogram (on the top and on the left of each graph) obtained by a hierarchical clustering based on similarities. (A) Similarities between the dent parental lines computed based on direct marker genotyping. (B) Similarities between the flint parental lines computed based on direct marker genotyping. (C) Similarities between the dent parental lines computed based on ancestral allele sharing (using clusthaplo and a 2-cM window size). (D) Similarities between the flint parental lines computed based on ancestral allele sharing (using clusthaplo and a 2-cM window size).

Figure S4). However, curves displaying evolution of –log10(*P*-values) along the genome were globally highly consistent across models and all models detected the same major QTL (Figure 3, Figure S1, Figure S2, Figure S3, and Figure S4). This was true even in cases when they detected a different number of QTL on the same chromosome. For instance, in the flint design, for DMC, all models detected a major QTL at 45–46 cM on chromosome 10 but two models detected other QTL in the region without challenging the position of the major QTL: the LDLA—2 cM model at 69.9 cM and the LDLA—1-marker model at 68.9 cM (Figure S1, Table S3, Table S4, Table S5, and Table S6).

Considering the QTL that were detected by different models, the ranking of the models according to their −log10(*P*-value) varied with the QTL. For instance, for the QTL detected with all models for DtSILK in the dent group at 70–74 cM on chromosome 6, the highest –log10(*P*-value) was found with the LDLA—2 cM model (17.5) and the lowest with the connected model (13) (Figure 3). In contrast, for the QTL detected with all models for DMY in the dent group on chromosome 6 at 14–17 cM, the highest −log10(*P*-value) was found with the connected model (14.9) (Figure S2 and Table S7) and the lowest with the LDLA—2 cM model (13.3) (Table S9).

Allelic effect series and comparison of the different allelic models for the major QTL detected for female flowering time

Visualization of allelic effects of the connected model through heat maps (Figure S5, Figure S6, Figure S7, Figure S8, Figure S9, Figure S10, Figure S11, Figure S12, Figure S13, and Figure S14) illustrated a continuous range of effects for all QTL. The central line had an intermediate value for most of the loci in both designs. Each parental line carried alleles with either positive or negative effects compared to the central line. LDLA models are expected to outperform the connected model if the clustering process correctly identifies underlying allelic series at QTL. To get further insight into this point, we compared allelic effects estimated by the different models for the two major DtSILK QTL found in this study.

Table 2 Number of QTL detected (Nb) and adjusted percentage of variance explained by the detected QTL (R^2) for the five traits in the two separate data sets for each model and for the joint data set for the connected model

	DMC		DMY		DtSILK		DtTAS		PH		Total	
	Nb	R^2 (%)	Nb	R^2 (%)	Nb	R^2 (%)	Nb	R^2 (%)	Nb	R^2 (%)	Nb	R^2 (%)
Dent												
Connected	12	51.4	8	32.7	11	52.3	7	41.2	14	57.1	52	46.9
LDLA—5 cM	15	51.1	5	22.5	12	53.7	11	49.2	13	54.1	56	46.1
LDLA—2 cM	16	53.6	6	23.4	12	53.2	9	45.1	12	49.5	55	45.0
LDLA—1-marker	12	37.4	5	18.6	11	43.2	7	33.3	10	36.4	45	33.8
Flint												
Connected	8	46.0	11	48.6	15	69.3	12	65.3	9	52.3	55	56.3
LDLA—5 cM	11	49.2	10	41.9	14	67.5	13	61.1	10	51.7	58	54.3
LDLA—2 cM	8	42.1	12	45.3	11	62.0	14	62.2	11	51.9	56	52.7
LDLA—1-marker	7	36.1	11	39.0	16	61.7	16	58.0	9	41.9	59	47.3
Joint												
Connected	18	54.6	16	45.5	15	59.7	17	61.4	21	61.2	87	56.5

We also indicated the total number of QTL detected over the traits and the average percentage of variance explained ("Total" column).

The allelic effects of the DtSILK major QTL detected in the flint group on chromosome 10 at 38–50 cM clearly showed an allelic series (Figure 4). The four models detected QTL in this region but at slightly different positions. For the QTL detected with the connected model, at least three classes of effects were identified based on *t*-tests. F283 and DK105 carried a late allele (3.7 and 3.5 days compared to UH007), UH006 an intermediate allele (2.07 days), and D152, UH009, F2, UH007, and F03802 an early allele (between −0.29 and 0.4 days), the three other parental lines showing effects between the early and the intermediate classes. For the QTL detected with the LDLA—5 cM and LDLA—2 cM models, allelic effects were globally consistent with those found for the QTL detected with the connected model except for EZ5, which had the earliest allele with the LDLA—5 cM model. Note that the family derived from this parent was one of the smallest of the design. The LDLA—1-marker model detected two QTL in this region: one at position 45.9 cM (close to the position of the QTL found with the other models) and one, of smaller effect, 7 cM apart at the position 38.6 cM. For the marker detected at position 45.9 cM, the late allele (2.44 days) was shared by F283, DK105 and UH006, which also carried the latest alleles according to the other models. All the other lines shared the same early allele (0 days). For the marker detected at position 38.6 cM, the late allele (1.1 days) was shared by DK105, F283 (the lines carrying the latest alleles in the other models), EC49A, and F64 (which carried alleles classified as intermediate). All the other lines shared the early allele (0 days). So, when considered jointly, these two markers account for the allelic series observed for the QTL detected with the other models: DK105 and F283 carrying the late alleles at the two markers, UH006 carrying the late allele for the marker with the strongest effect and the early allele for the other marker, EC49A and F64 carrying the late allele at the marker with the smallest effect and the early allele for the other one, and D152, UH009, F2, UH007, and F03802 carrying at both markers the early alleles. The two QTL detected with the LDLA—1-marker model individually explained 2.2 and 11.1% of the variance for the marker at positions 38.6 and 45.9 cM, respectively, but they jointly explained 26.8% of the variance, only slightly less than the variance explained by the QTL detected with the other models (between 27.5 and 28.2%).

The allelic effects of the DtSILK QTL detected in the dent group, on chromosome 8 at 45–58 cM also clearly showed an allelic series and the same type of pattern (Figure 5). With the connected model, allelic effects showed a continuous variation and at least two classes of alleles could be identified. Four inbred lines (D06, D09, UH250, and F618) carried early alleles compared to the group consisting of F353 (central line), EC169, and Mo17. The other parental alleles were not clearly classified but had intermediate effects. In this chromosome region, the two LDLA models based on ancestral allele clustering both identified a QTL. With both window sizes, D06, D09, and UH250, which carried the earliest alleles in the connected model, were attributed to the same ancestral allele with an early effect (−1.77 with LDLA—5 cM and −1.76 with LDLA—2 cM compared to F353). Mo17, EC169 (the two lines with latest allelic effects in the connected model), UH304, and F353 were attributed to the same or to different ancestral alleles depending on the window size but in both cases their allelic effects were equal or close to zero. With these models, B73 was attributed the latest effect (0.4 or 0.49) but this effect was not significantly different from zero. The other lines had allelic effects consistent with the effects estimated with the connected model. Two QTL were detected in this region with the LDLA—1-marker model: one at 45.5 cM and the other at 57.3 cM, on either side of the QTL detected with the other models. D06, D09, and UH250, which carried the earliest allele of the connected model and were attributed to the same early ancestral allele with LDLA—2 cM and LDLA—5 cM models, carried the early allele at both QTL. Mo17, EC169, B73, and F353, the lines with the latest allelic effects with the other models, carried the late allele at both QTL. The other lines, which had intermediate allelic effects with the other models, carried the late allele at one QTL and the early allele at the other QTL.

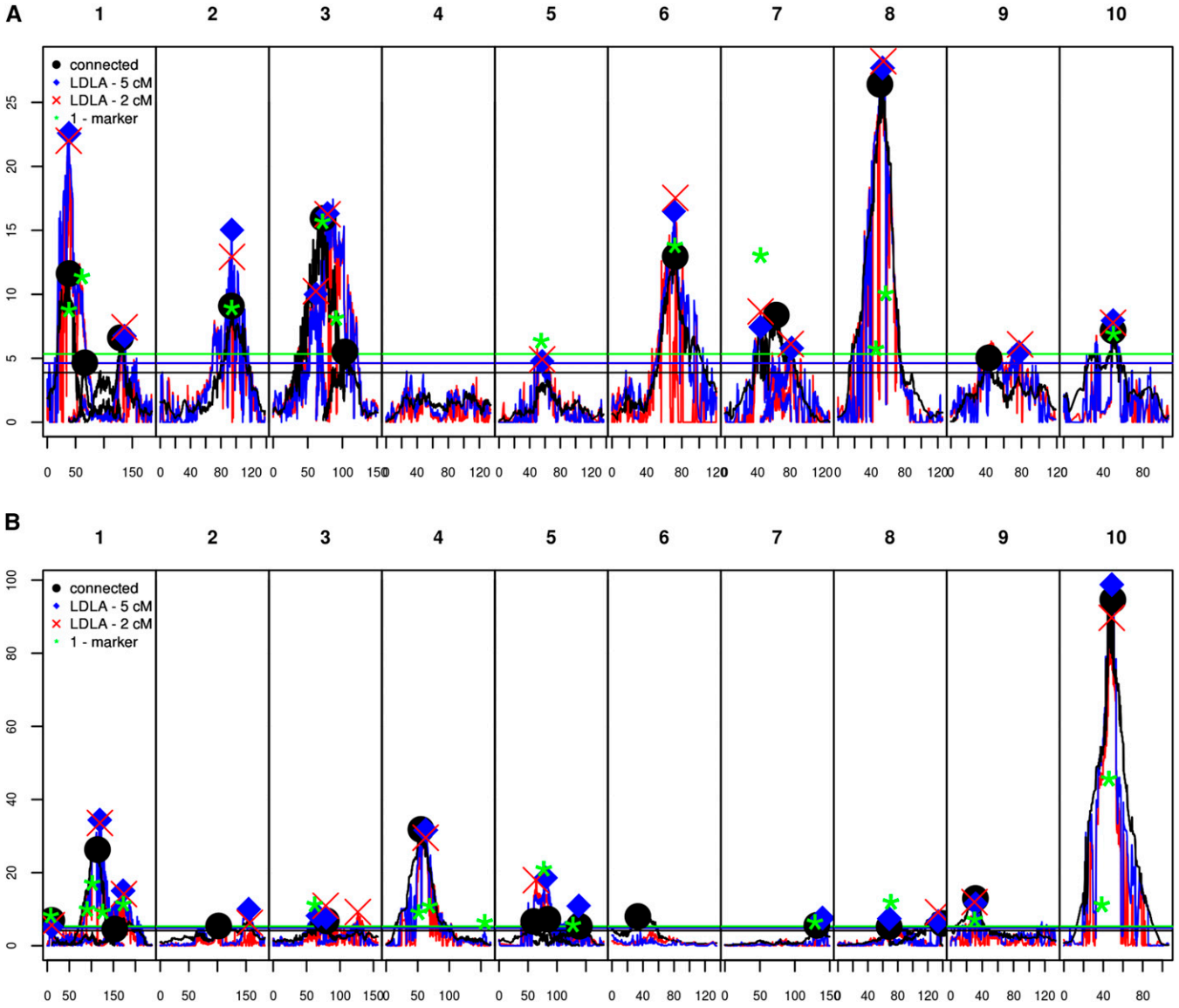

Figure 3 Results of the QTL detection with each model for DtSILK for (A) the dent design and (B) the flint design. The −log10(*P*-values) of the connected model are represented by black lines, the QTL positions of the connected models by black dots. The −log10(*P*-values) of the LDLA—5 cM model are represented by blue lines and the QTL positions by blue diamonds. The −log10(*P*-values) of the LDLA—2 cM model are represented by red lines and the QTL positions by red crosses. The −log10(*P*-values) of the QTL detected by the LDLA—1-marker model are represented by green stars. Horizontal lines correspond to the threshold values of the different models.

Thus, marker effects at these two QTL jointly mimic the allelic series identified by the other models. The two QTL detected with the LDLA—1-marker individually explained 1.5 and 2.9% of the variance but they jointly explained 7.9% of the variance, which is only slightly less than the other models (8.9% for the LDLA—5 cM and LDLA—2-cM models and 9.6% for the connected model).

Comparison of the QTL detected in the two heterotic groups analyzed individually and jointly

In total, for the connected model, 52 QTL were detected in the dent design for all traits and 55 in the flint design (Table 2). More QTL were found in the dent than in the flint design for DMC and PH, whereas the reverse was observed for DtSILK, DtTAS, and DMY.

Based on overlap of their confidence intervals, when comparing results obtained in the two separate data sets, only seven QTL were common between the two groups. Two of these QTL were for DMC (chromosomes 8 and 10), three for DtSILK (chromosomes 1, 2 and 3), one for DtTAS (chromosome 3), and one for PH (chromosome 1). No common QTL were found for DMY. In addition, some chromosome regions carried QTL detected in the two groups but not for the same trait (Figure 6).

The distribution of QTL effects (in terms of R^2) differed in the two groups (Figure 7). In the dent group, all the QTL

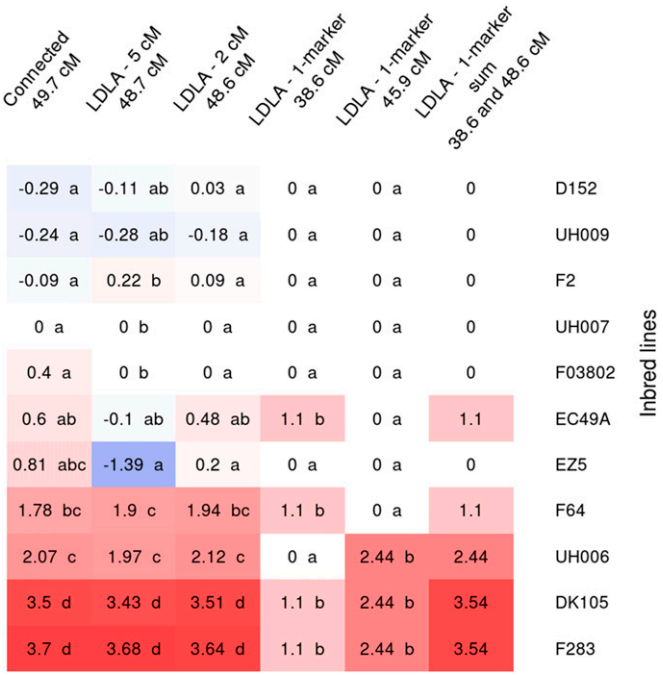

Figure 4 Allelic effects for the different flint lines for the QTL detected on chromosome 10 at 38–50 cM for DtSILK with all the QTL detection models. Allelic effects are estimated in contrast to the central line allelic effect (UH007), which was set to zero. The same letter was given to allelic effects not significantly different at a 5% risk level. Alleles with intermediate effects may be attributed to more than one letter. The last column corresponds to the joint effect of the two QTL detected in the region with LDLA—1-marker model. Allelic effects estimated for EP44 were not shown because the population where it segregates was too small (17 individuals) to obtain a reliable estimation. Inbred lines are ranked according to their allelic effects obtained with the connected model.

had low to medium effect ($R^2 < 10\%$). The QTL with the biggest effect was detected on chromosome 3 at 63 cM for DtTAS and explained 10.4% of the variance (Table S7). A QTL was also detected at this position for DMC but with a smaller effect. The second biggest QTL was detected on chromosome 8 at position 50 cM for DtSILK and explained 9.4% of the genetic variance. This region was also detected for the other traits but with smaller effects. On the contrary, in the flint group, one region located on chromosome 10 around position 44–50 cM showed a major effect on all the traits (Table S3). Depending on the trait considered, this region explained between 14% of the variation for DMY and 27.5% for DtSILK. All the other QTL detected in this group showed milder effects with $R^2 < 10\%$. It is interesting to note that the QTL that exhibited a strong effect in one group (the QTL detected on chromosome 10 in the flint group and the QTL detected on chromosome 3 and 8 in the dent group) did not have such a strong effect in the other group for the same traits.

Eighty-seven QTL were detected in total with the joint analysis, which is less than the sum of the QTL found in the two separate data sets (107) (Table 2 and Table S11). For each trait, the number of QTL detected with the joint analysis was equal or superior to that detected in each single data set analysis. For DMC and PH, QTL detected with the joint analysis explained a larger fraction of variance than the one explained in the separate data sets analysis. On the contrary, for DMY, DtSILK, and DtTAS, more variance was explained in the flint data set analysis than in the joint analysis.

QTL found in the joint analysis were generally found at the same position or close to QTL detected in one or both separate analyses (Figure 6). In some cases, they were detected between two QTL detected in a single data set analysis (for instance, QTL on chromosome 5 for DtSILK), or between one QTL detected in the dent data set and one detected in the flint data set (QTL at 130 cM on chromosome 2 for DMC). In some cases, no QTL was detected with the joint analysis although QTL were detected in the separate data sets (for instance flint QTL at 9 cM on chromosome 1 or dent QTL on chromosome 2 for DtTAS). Other QTL were detected only with the joint analysis (and not close to or between two QTL detected with the separate analysis), as the one detected for DMC on chromosome 7.

When testing the effects of these 87 QTL in the separate data sets, 30 were significant in both data sets, 52 in a single data set only, and 5 in none of the data sets (Table 3). So the number of QTL with effect in both data set varied between 27% for DtSILK and 41% for DtTAS.

Concerning the seven QTL found common when comparing the dent and flint separate analyses, the joint analysis always found a QTL in the region nearby (not necessarily with overlapping of the confidence regions but really close). Except for the QTL found on chromosome 2 for DtSILK, these QTL were significant in both groups.

Discussion

Our study aimed at comparing genetic determinism of biomass related traits in two complementary flint and dent genetic pools that are often used to produce commercial hybrids in Northern Europe. To do so, a new NAM DH population was developed for each group. Both NAM populations display intermediate levels of diversity compared to the U.S. NAM design and classical elite breeding programs. Data from each design were analyzed with four models: a connected model where parents are assumed to carry different alleles, an LDLA model based on single-marker information close to the one successfully used for the U.S. NAM design, and two LDLA models based on ancestral allele modeling previously used with success by Leroux *et al.* (2014) and Bardol *et al.* (2013). In addition, data of the two designs were analyzed jointly with the connected model, considering that the central line of one design was used as tester in the other design and reciprocally.

Linkage disequilibrium and clustering of parental alleles

The haplotype clustering approach of Leroux *et al.* (2014) requires the definition of a window size according to genetic map units (centimorgans, cM). We defined it based on the

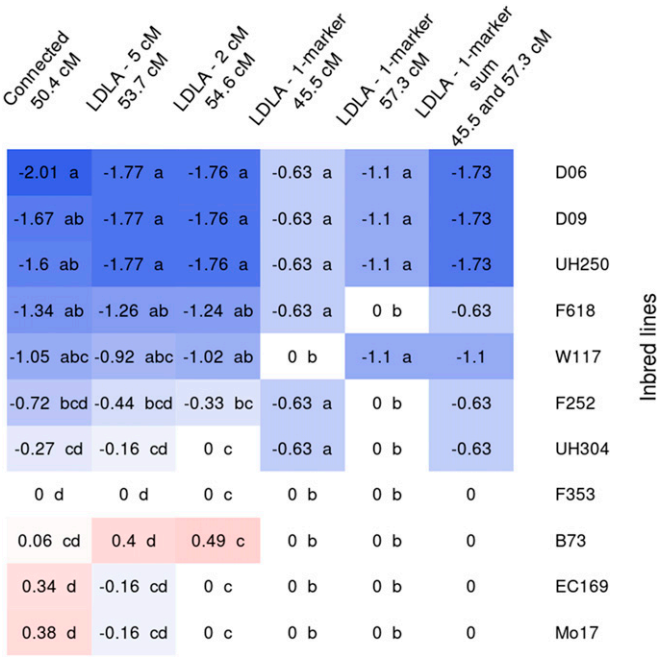

Figure 5 Allelic effects for the different dent lines for the QTL detected on chromosome 8 at 45–58 cM for DtSILK with all the models. Allelic effects are estimated in contrast to the central line allelic effect (F353), which was set to zero. The same letter was given to allelic effects not significantly different at a 5% risk level. Alleles with intermediate effects may be attributed to more than one letter. The last column corresponds to the joint effect of the two QTL detected in the region with LDLA—1-marker model. Inbred lines are ranked according to their allelic effects obtained with the connected model.

estimation of the LD extent at the level of the parental lines. This showed that LD decreased below $r^2 = 0.2$ after ~1 and 2 cM in the flint and dent parental lines, respectively. Although estimated with only 11 and 12 inbred lines, for the dent and flint group respectively, these values were consistent with the LD extent observed for these groups by van Inghelandt *et al.* (2011). Based on this result, we considered two window sizes for the parental clustering, one of 2 cM, more adapted to the flint group and one of 5 cM, more adapted to the dent group. Note that a 1 cM window was also considered but the HMM approach did not converge with the R version we used for this study. These values are smaller than the 10-cM window size used in Bardol *et al.* (2013) to analyze a multiparental design derived from highly related founders.

In both flint and dent groups, the clustering process identified on average six and seven ancestral alleles per position for the 2- and 5-cM window sizes, respectively. The percentage of genome detected as IBD was in agreement with the marker-based similarities between inbred line pairs and pedigree information. These results showed that among dent lines, there were two groups of related lines: (i) D09, D06, and UH250, which came from the breeding program of the University of Hohenheim, and (ii) UH304 and F353, which share a common Iodent background (Bauer *et al.* 2013). For the flint, there was a separation between EC49A, EZ5, EP44 (the three lines with Spanish origin), and F64 (Argentinean origin) and all the other lines.

The number of ancestral alleles detected after clustering with clusthaplo varied along the genome, first at the local level, from one position to the next. This results in a variation in model dimension along the genome that certainly explains the erratic pattern of the –log10(*P*-values) curves of the LDLA models (see below). Beyond this local variation we observed that on average more ancestral alleles were detected in the centromeric than in the telomeric regions. This result is probably related to the higher number of marker loci per centimorgan in centromeric regions than in telomeric ones. It may be also related to a higher divergence between lines in centromeric regions. The similarity score used in clusthaplo is expected to be robust against the difference of marker density inside the sliding windows (Leroux *et al.* 2014). Our results suggest, however, that we reached the limits in this robustness. As most of the lines were not closely related, the size of IBD segments was expected to be limited, which made them difficult to detect. Visual inspection of the graphs of IBD segments (results not shown) indeed revealed that the segments were in general shorter than in Bardol *et al.* (2013) except for related lines such as D06 and D09. The method implemented in the clusthaplo software should therefore be adapted to cope with more diverse sets of lines than the one considered in Leroux *et al.* (2014), possibly by reducing window sizes in regions of the genome where marker density is high and local LD is low relative to the genetic map.

Adapting the method to cope with populations with limited LD also raises issues regarding the genetic map to be considered for the clustering process. Bauer *et al.* (2013) showed that even if the individual maps of the families of a given group had globally consistent order, putative inversions were found in some areas. This is in agreement with recent studies that showed copy-number variations (Springer *et al.* 2009; Swanson-Wagner *et al.* 2010), chromosomal inversions, or translocations between the different maize lines. Ganal *et al.* (2011) also suggested that some regions of the physical map of B73 v. 2 are not correctly assembled. This may have affected our consensus maps since information from the physical map was used for positioning the markers and this may have affected the clustering process. It appears thus important to further evaluate the properties of the clustering approach when using denser genotyping data and also evaluate its potential interest in the context of the rapid emergence of sequencing data that may enable a more direct identification of conserved haplotypes between inbred lines.

Comparison of the different QTL detection models

The highest total number of QTL was detected by one of the three LDLA models in both designs. We noted, however, different trends for the two designs. For the dent, LDLA—2 cM and LDLA—5 cM detected very similar numbers of QTL (55 and 56, respectively), more than for both the connected

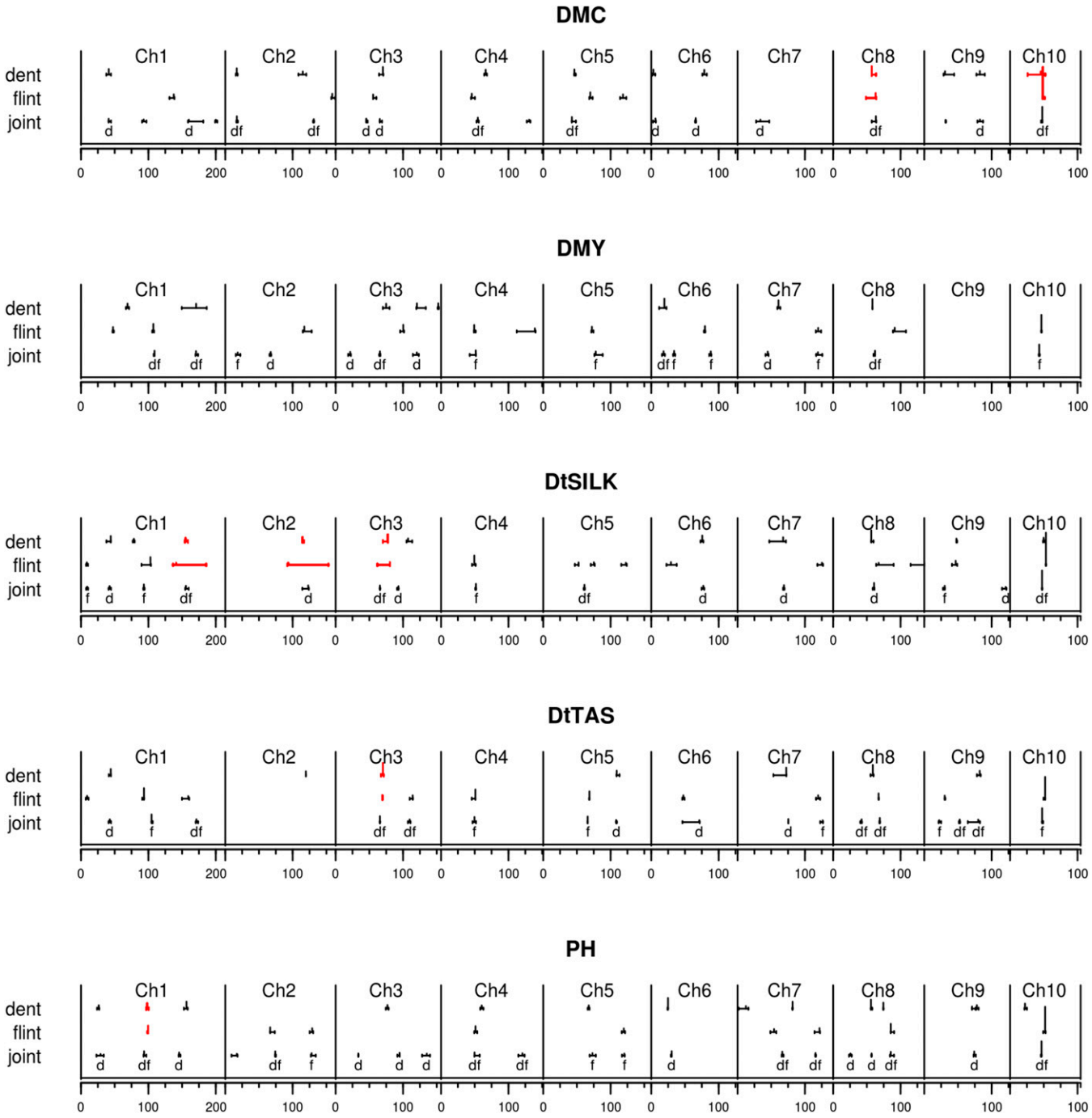

Figure 6 QTL projection on the flint–dent consensus map of the QTL detected in the dent data set, the flint data set, and the joint data set for DMC, DMY, DtSILK, DtTAS, and PH. Each QTL is displayed by one horizontal line bound by two vertical lines representing the confidence region and a vertical line proportional to the QTL adjusted R^2 symbolizing the QTL position. QTL common to dent and flint according to the overlap of their confidence region on the dent–flint consensus map are represented in red. For the QTL detected in the joint analysis, the letters d and f written below the QTL indicate that the QTL was significant when tested in the dent or flint data set respectively.

and LDLA—1-marker models (52 and 45, respectively). Note that Bardol *et al.* (2013) also found that in an elite dent breeding pool, the LDLA method based on ancestral alleles detected on average more QTL than the LDLA—1-marker model. Our results suggest that the genotyping data and window sizes used for clusthaplo were well suited for LDLA models for the dent design. For the flint design, the connected model detected fewer QTL (55) than the LDLA—5 cM, the LDLA—2 cM and the 1-marker model (58, 56, and 59 respectively), but differences between models were small on average This suggests that the available density of genotyping data and/or window size we could use with

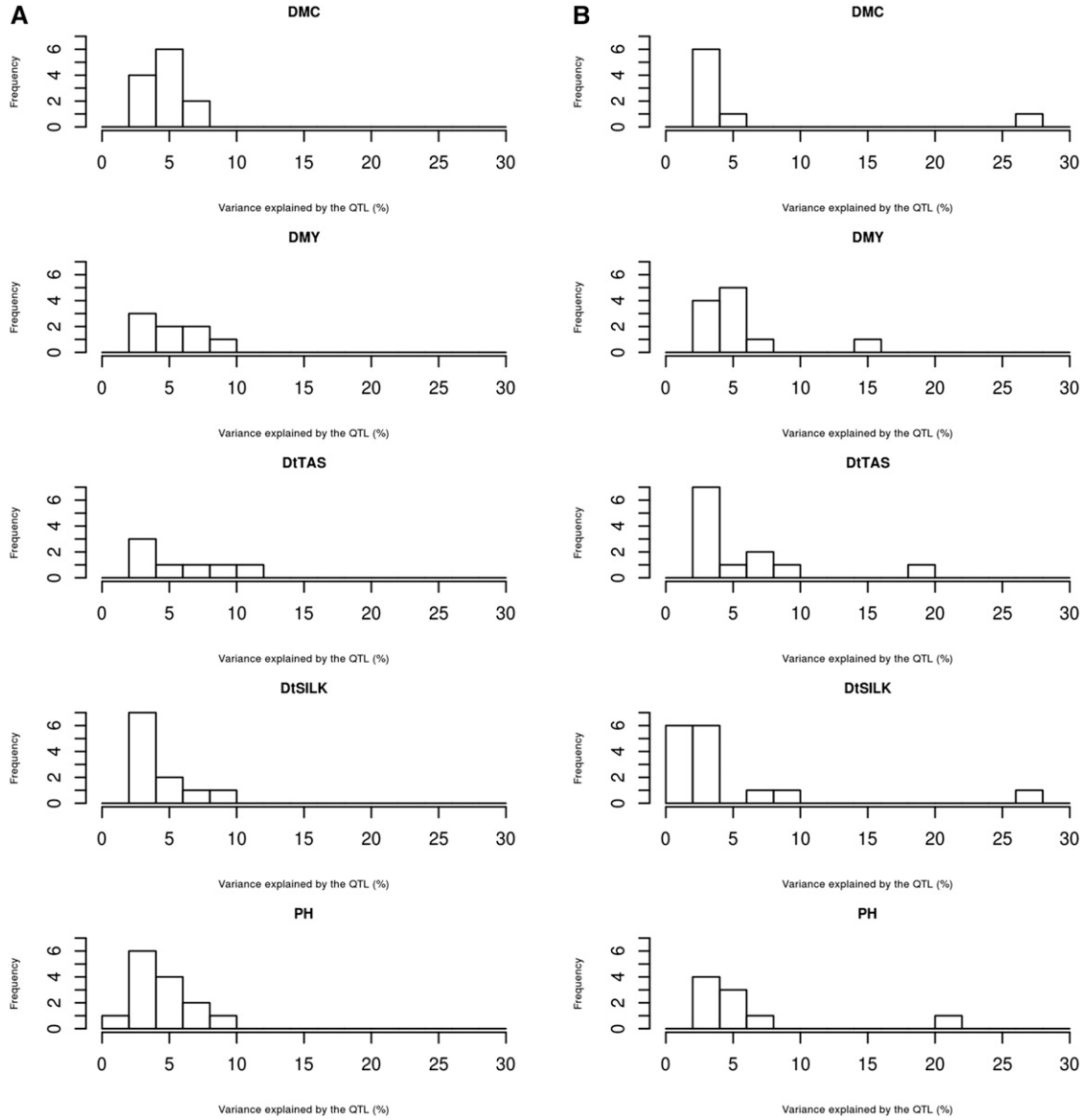

Figure 7 Distribution of the percentage of variance (R^2_{QTL}) explained by the QTL detected in (A) the dent design and (B) the flint design, with the connected model and for the five traits.

the HMM approach were not necessarily optimal for this design. Interestingly, although the connected model was globally outperformed by LDLA models in terms of number of QTL detected, it explained a higher percentage of variance than the other models for nearly all the traits. Conversely, the LDLA—1-marker model explained a smaller percentage of variance even when detecting more QTL. As the estimations of the percentages of variation explained were adjusted for the number of parameters, this cannot be due to model overfitting. One can thus hypothesize that a large part of the QTL showed allelic series that are not completely accounted for by local similarities or single-marker information. This is consistent with Würschum *et al.* (2012) who compared by simulation different models for joint linkage association mapping. They concluded that, even if the single SNP model was more powerful in terms of detection, the model considering one allele per parent was better adapted to estimate QTL effects in case of multiallelic series, corroborating experimental results of Liu *et al.* (2011).

Globally, LDLA models and linkage analysis detected QTL in the same chromosome regions although fine comparison of QTL positions was complicated by the relatively noisy pattern of the LDLA $-\log10(P\text{-value})$ curves. We noted that the number of QTL in a given genomic region could either be the same or vary across models. In cases when a single QTL position is detected by all models, one can assume that variation is most likely due to a single QTL with two alleles well reflected by a single biallelic marker. On the opposite, a variable number of QTL across models suggests a more complex situation with linkage between several QTL or

Table 3 Number of QTL detected for the five traits in the joint data set for the connected model and found significant in each separate data set, in both separate data sets and in none of the separate data set

	DMC	DMY	DtSILK	DtTAS	PH	Total
Significant in the whole data set (Nb)	18	16	15	17	21	87
Significant in the dent data set (Nb)	14	9	11	11	17	62
Significant in the flint data set (Nb)	6	12	8	13	11	50
Significant in both data sets (Nb)	6	5	4	7	8	30
Non significant in both data sets (Nb)	4	0	0	0	1	5

allelic series at a single QTL. This can be exemplified by the DtSILK QTL detected on chromosome 8 in the dent design. In this region, the LDLA—1-marker model detected two QTL 12 cM apart and located on both sides of the single QTL detected with the connected model. This suggests that either the two marker loci were needed to account for the allelic series at a single QTL or conversely that the connected model failed at distinguishing the two underlying QTL due to limited recombination in DH families.

The different models thus showed variable efficiency depending on the trait and region considered, which highlights complementarities of different allele coding methods in deciphering allelic series in genetic studies.

Comparison between the QTL detected in the two heterotic groups and evolutionary interpretation

Similar numbers of QTL were detected in the two groups with the separate data set analyses, showing that both can contribute genetic variation useful for breeding in Northern Europe. Less than 15% of the QTL was common between the dent and flint design when comparing the positions of the QTL detected in the separate data set analyses. This is consistent with the long time divergence between the dent and flint heterotic groups: >500 years (Tenaillon and Charcosset 2011). Part of this low value can be due to power issues. Indeed the joint analysis enabled us to detect additional QTL compared to single group analysis and among the detected QTL with the joint analysis, 34% on average were significant in both groups. However, some QTL detected in individual designs disappeared in the joint analysis, which suggests that they were really specific of one group and that variation within the other group diminished power at these QTL in the joint analysis. Some of the QTL detected in the joint analysis were found at an intermediate position between the positions of design-specific QTL. This may correspond to a gain in precision but one cannot exclude that these QTL might also correspond to an artifact "ghost" QTL between actual QTL.

Note that in addition to the common QTL, some chromosome regions had an effect in both designs but for different traits. These QTL could be pleiotropic QTL for which effects on some traits were not detected in one of the designs, due to a lack of power, diversity, etc.

When comparing the single data set analyses, QTL common to flint and dent designs were observed for DMC, DtSILK, DtTAS, and PH. It is interesting to note that no common QTL was observed for DMY. With the joint analysis, the percentage of QTL significant in both data sets was smaller for DtSILK and DMY (27 and 31%, respectively) than for the other traits (33% for DMC to 41% for DtTAS). For traits subjected to directional selection such as DMY, several alleles must have been fixed over time but there is no reason that the same alleles were fixed in both groups, especially considering that selection for hybrid value certainly favored fixation of complementary alleles in each group (Schön *et al.* 2010; Larièpe *et al.* 2012). This may explain why only few common QTL or QTL significant in both groups were detected for DMY. On the contrary, for traits for which a stabilizing selection is performed, the same polymorphisms are more likely to be maintained in both groups. This is the case for PH and DtTAS and also indirectly for DMC since DMC at harvest of a genotype depends on its precocity and its drying speed. Interestingly, common DMC QTL between groups and most of the DMC QTL detected with the joint analysis and significant in both data sets were detected in regions also carrying QTL for flowering time (DtSILK or DtTAS).

The few common QTL between dent and flint groups that we detected could explain the low predictive abilities of the prediction between dent and flint in genomic selection (Meuwissen *et al.* 2001; Jannink *et al.* 2010) when dent are in the estimation set and flint in the test set and *vice versa* (Lehermeier *et al.* 2014). The presence of a major effect QTL in the flint group might also partly explain this result.

Overview of detected QTL and comparison with literature studies

For the single data set analyses, between 20 QTL for DMY and 28 QTL for DtSILK were detected in total over the two groups when considering the model that detected the highest number of QTL. For the joint analysis, between 15 QTL for DtSILK and 21 QTL for PH were detected.

For DtSILK, although high, the number of detected QTL is less than the one reported for the U.S. NAM design (39 QTL detected with the multiple family joint stepwise model, 52 with JCIM) (Buckler *et al.* 2009; Li *et al.* 2011). This is also less than the total number of QTL estimated through meta-analysis for flowering time (62 and 59 in Chardon *et al.* 2004 and Salvi *et al.* 2009, respectively). QTL detected in our study explained a smaller proportion of the variance (for the connected model the detected QTL explained 52.3%, for the dent design, 59.7% for the joint analysis, and 69.3%, for the flint design of the within family variability) than the one detected on the U.S. NAM design (89%) (Buckler *et al.* 2009; Li *et al.* 2011). Similar trends were observed for male flowering (DtTAS). In our study, all QTL explained 10% or less of variation, with the exception of the main QTL found in the flint design on chromosome 10 (45–50 cM with the

connected model). In the joint analysis, this QTL was significant for female flowering when tested in both data sets, whereas for male flowering it was significant only in the flint data set. This QTL was also found by Blanc *et al.* (2006) and is close to the *ZmCCT* gene, which was fine mapped as a major flowering time QTL by Ducrocq *et al.* (2009) and validated by Coles *et al.* (2011). In the flint design, for the connected model, this QTL explained 18.7 and 27.5% of male and female flowering time, respectively. In the joint analysis, it explained 12 and 15.2% of male and female flowering time, respectively. This value is higher than that reported for the same region in the U.S. NAM (1.1% for male flowering and 1.3% for female flowering with joint linkage stepwise model in Buckler *et al.* 2009) and in Blanc *et al.* (2006) (18% for female flowering). These differences can be explained by the fact that several lines in our flint design share a late allele and possibly suggest that the expression of the effect of this QTL is amplified in early flowering backgrounds compared to the later U.S. NAM background. In the dent design analyzed separately, the most significant DtSILK QTL was found on chromosome 8. This QTL does not seem to be located in the region where two major flowering time QTL, *vgt1* and *vgt2* (*ZCN8*), have been fine mapped (Salvi *et al.* 2007; Bouchet *et al.* 2013). It seems to be close to an area where other studies also found QTL for flowering time (Ducrocq *et al.* 2008; Salvi *et al.* 2009; Bouchet *et al.* 2013).

For plant height (PH), we detected in total 25 QTL, which explained 55.0 and 57.1% of the variation for the flint and dent designs, respectively. With the joint analysis, we detected 21 QTL, which explained 61.2% of the variation. A recent study (Peiffer *et al.* 2014) based on the U.S. NAM and IBM family (Lee *et al.* 2002) reported 89 family-nested markers detected with an adaptation of JCIM and 277 associations through a joint-linkage-assisted genome-wide association study (Tian *et al.* 2011). Except the QTL found on chromosome 10 in the flint design and that likely corresponds to a pleiotropic effect of a major flowering time QTL, no QTL explained >10% of the variation, in the separate or joint data sets. As in Peiffer *et al.* (2014), none of the QTL detected in this study seem to be located in the vicinity of known candidate genes for plant height.

For DMY, with the separate analyses, we detected in total 20 QTL, which is lower than the number of QTL detected for the other traits. With the joint analysis, we detected 16 QTL, which is one of the lowest number of QTL detected. This may be explained by the lower heritability of this trait and the fact that variation for this trait may involve numerous QTL of small effects that are difficult to detect. For DMC, we detected in total 27 QTL with the separate analyses and 18 with the joint analysis. Only few studies address QTL detection for biomass yield and dry matter content, mainly in biparental populations (*e.g.*, Lübberstedt *et al.* 1998; Méchin *et al.* 2001; Barriere *et al.* 2010; Barriere *et al.* 2012). They reported only limited number of QTL and are not easily comparable with our results. Our study, which led to the detection of many QTL in a multiparental context, therefore represents a large advance toward understanding the genetics of biomass yield.

Thus globally, although high compared to the number of QTL indentified in biparental populations, the number of QTL detected in this study appears lower than those detected in most comprehensive designs and meta-analysis. Several explanations can be given for this result. First, compared with the U.S. NAM design, our experimental designs explore less diversity and included fewer individuals (841 and 811 DH lines for the dent and flint designs, respectively, compared to 5000 RILs for the U.S. NAM design). Moreover, as DH lines were used instead of RILs, the number of recombination events in our designs is expected to be two times lower per family. This certainly affected the power and resolution of our designs for deciphering trait variation even with LDLA models. One cannot exclude that QTL detected in our study may indeed correspond to clusters of linked QTL that could have been individually detected using a higher number of individuals, a higher number of markers and progenies exhibiting more crossovers (Huang *et al.* 2010). The main specificity of our study compared to the U.S. NAM design was that the different families were evaluated through their testcross progeny to evaluate traits related to biomass production at usual productivity levels. Under the hypothesis of additivity, the genetic variance is expected to be four times lower for testcross value than for *per se* value. In addition, the two central lines of each group that were used as testers for the other group belong to two complementary heterotic pools, so one expects to observe some dominance effects between the flint and the dent alleles at QTL. Such dominance effects may have masked part of the variability in each group. Despite these limitations, as progenies were evaluated based on testcross performance, the QTL detected in this study directly reflect the genetic variation present in each of the two main heterotic groups that is useful for breeding in European conditions.

Acknowledgments

Results have been achieved within the framework of the Transnational Cooperation within the PLANT-KBBE Initiative CornFed, with funding from the Federal Ministry of Education and Research (BMBF, Germany), Agence Nationale de la Recherche (ANR, France), and Ministry of Science and Innovation (MICINN, Spain). Part of this research was funded by the Federal Ministry of Education and Research (BMBF, Germany) within the Agro-ClustEr Synbreed-Synergistic plant and animal breeding (FKZ 0315528A).

Literature Cited

Bardol, N., M. Ventelon, B. Mangin, S. Jasson, V. Loywick *et al.*, 2013 Combined linkage and linkage disequilibrium QTL mapping in multiple families of maize (*Zea mays* L.) line crosses highlights complementarities between models based on parental haplotype and single locus polymorphism. Theor. Appl. Genet. 126: 2717–2736.

Barriere, Y., V. Mechin, D. Denoue, C. Bauland, and J. Laborde, 2010 QTL for yield, earliness, and cell wall quality traits in topcross experiments of the F838 × F286 early maize RIL progeny. Crop Sci. 50: 1761–1772.

Barriere, Y., V. Méchin, B. Lefevre, and S. Maltese, 2012 QTLs for agronomic and cell wall traits in a maize RIL progeny derived from a cross between an old Minnesota13 line and a modern Iodent line. Theor. Appl. Genet. 125: 531–549.

Bauer, E., M. Falque, H. Walter, C. Bauland, C. Camisan *et al.*, 2013 Intraspecific variation of recombination rate in maize. Genome Biol. 14: R103.

Bink, M. C. A. M., L. R. Totir, C. J. F. ter Braak, C. R. Winkler, M. P. Boer *et al.*, 2012 QTL linkage analysis of connected populations using ancestral marker and pedigree information. Theor. Appl. Genet. 124: 1097–1113.

Blanc, G., A. Charcosset, B. Mangin, A. Gallais, and L. Moreau, 2006 Connected populations for detecting quantitative trait loci and testing for epistasis: an application in maize. Theor. Appl. Genet. 113: 206–224.

Bouchet, S., B. Servin, P. Bertin, D. Madur, V. Combes *et al.*, 2013 Adaptation of maize to temperate climates: mid-density genome-wide association genetics and diversity patterns reveal key genomic regions, with a major contribution of the Vgt2 (ZCN8) locus. PLoS ONE 8: e71377.

Browning, B. L., and S. R. Browning, 2009 A unified approach to genotype imputation and haplotype-phase inference for large data sets of trios and unrelated individuals. Am. J. Hum. Genet. 84: 210–223.

Buckler, E. S., J. B. Holland, P. J. Bradbury, C. B. Acharya, P. J. Brown *et al.*, 2009 The genetic architecture of maize flowering time. Science 325: 714–718.

Charcosset, A., and A. Gallais, 1996 Estimation of the contribution of quantitative trait loci (QTL) to the variance of a quantitative trait by means of genetic markers. Theor. Appl. Genet. 93: 327–333.

Charcosset, A., M. Causse, L. Moreau, and A. Gallais, 1994 Investigation into effect of genetic background on QTL expression using three connected maize recombinant inbred lines (RIL) populations, pp. 75–84 in *Biometrics in plant breeding: applications of molecular markers: Proceedings of the 9th Meeting of the Eucarpia Section Biometrics in Plant Breeding*, edited by J. W. van Oijen and J. Jansen. Wageningen, The Netherlands.

Charcosset, A., B. Mangin, L. Moreau, L. Combes, M.-F. Jourjon *et al.*, 2000 Heterosis in maize investigated using connected RIL populations, pp. 89–98 in *Quantitative Genetics and Breeding Methods: The Way Ahead*, edited by A. Gallais, C. Dillman, and I. Goldringer. INRA, Paris, France.

Chardon, F., B. Virlon, L. Moreau, M. Falque, J. Joets *et al.*, 2004 Genetic architecture of flowering time in maize as inferred from quantitative trait loci meta-analysis and synteny conservation with the rice genome. Genetics 168: 2169–2185.

Coles, N. D., C. T. Zila, and J. B. Holland, 2011 Allelic effect variation at key photoperiod response quantitative trait loci in maize. Crop Sci. 51: 1036–1049.

Cook, J. P., M. D. McMullen, J. B. Holland, F. Tian, P. Bradbury *et al.*, 2012 Genetic architecture of maize kernel composition in the nested association mapping and inbred association panels. Plant Physiol. 158: 824–834.

Ducrocq, S., D. Madur, J.-B. Veyrieras, L. Camus-Kulandaivelu, M. Kloiber-Maitz *et al.*, 2008 Key impact of Vgt1 on flowering time adaptation in maize: evidence from association mapping and ecogeographical information. Genetics 178: 2433–2437.

Ducrocq, S., C. Giauffret, D. Madur, V. Combes, F. Dumas *et al.*, 2009 Fine mapping and haplotype structure analysis of a major flowering time quantitative trait locus on maize chromosome 10. Genetics 183: 1555–1563.

Frascaroli, E., T. A. Schrag, and A. E. Melchinger, 2013 Genetic diversity analysis of elite European maize (*Zea mays* L.) inbred lines using AFLP, SSR, and SNP markers reveals ascertainment bias for a subset of SNPs. Theor. Appl. Genet. 126: 133–141.

Ganal, M. W., G. Durstewitz, A. Polley, A. Bérard, E. S. Buckler *et al.*, 2011 A large maize (*Zea mays* L.) SNP genotyping array: development and germplasm genotyping, and genetic mapping to compare with the B73 reference genome. PLoS ONE 6: e28334.

Gore, M. A., J.-M. Chia, R. J. Elshire, Q. Sun, E. S. Ersoz *et al.*, 2009 A first-generation haplotype map of maize. Science 326: 1115–1117.

Hill, W. G., and A. Robertson, 1968 Linkage disequilibrium in finite populations. Theor. Appl. Genet. 38: 226–231.

Hill, W. G., and B. S. Weir, 1988 Variances and covariances of squared linkage disequilibria in finite populations. Theor. Popul. Biol. 33: 54–78.

Huang, X., X. Wei, T. Sang, Q. Zhao, Q. Feng *et al.*, 2010 Genome-wide association studies of 14 agronomic traits in rice landraces. Nat. Genet. 42: 961–967.

Jannink, J. L., A. J. Lorenz, and H. Iwata, 2010 Genomic selection in plant breeding: from theory to practice. Brief. Funct. Genomics 9: 166–177.

Jansen, R. C., J.-L. Jannink, and W. D. Beavis, 2003 Mapping quantitative trait loci in plant breeding populations: use of parental haplotype sharing. Crop Sci. 43: 829–834.

Jourjon, M.-F., S. Jasson, J. Marcel, B. Ngom, and B. Mangin, 2005 MCQTL: multi-allelic QTL mapping in multi-cross design. Bioinformatics 21: 128–130.

Kump, K. L., P. J. Bradbury, R. J. Wisser, E. S. Buckler, A. R. Belcher *et al.*, 2011 Genome-wide association study of quantitative resistance to Southern leaf blight in the maize nested association mapping population. Nat. Genet. 43: 163–168.

Lander, E. S., and D. Bolstein 1989 Mapping mendelian factors underlying quantitative traits using RFLP linkage maps. Genetics 121: 185–199.

Larièpe, A., B. Mangin, S. Jasson, V. Combes, F. Dumas *et al.*, 2012 The genetic basis of heterosis: multiparental quantitative trait loci mapping reveals contrasted levels of apparent overdominance among traits of agronomical interest in maize (Zea mays L.). Genetics 190: 795–811.

Lee, M., N. Sharopova, W. D. Beavis, D. Grant, M. Katt *et al.*, 2002 Expanding the genetic map of maize with the intermated B73 × Mo17 (IBM) population. Plant Mol. Biol. 48: 453–461.

Lehermeier, C., N. Krämer, E. Bauer, C. Bauland, C. Camisan *et al.*, 2014 Usefulness of multi-parental populations of maize (*Zea mays* L.) for genome-based prediction of testcross performance. Genetics 198: 3–16.

Leroux, D., A. Rahmani, S. Jasson, M. Ventelon, F. Louis *et al.*, 2014 Clusthaplo: a plug-in for MCQTL to enhance QTL detection using ancestral alleles in multi-cross design. Theor. Appl. Genet. 127: 921–933.

Li, H., P. Bradbury, E. Ersoz, E. S. Buckler, and J. Wang, 2011 Joint QTL linkage mapping for multiple-cross mating design sharing one common parent. PLoS ONE 6: e17573.

Li, J., and T. Jiang, 2005 Haplotype-based linkage disequilibrium mapping via direct data mining. Bioinformatics 21: 4383–4393.

Liu, W., M. Gowda, J. Steinhoff, H. P. Maurer, T. Würschum *et al.*, 2011 Association mapping in an elite maize breeding population. Theor. Appl. Genet. 123: 847–858.

Liu, W., J. C. Reif, N. Ranc, G. D. Porta, and T. Würschum, 2012 Comparison of biometrical approaches for QTL detection in multiple segregating families. Theor. Appl. Genet. 125: 987–998.

Lübberstedt, T., A. E. Melchinger, S. Fahr, D. Klein, A. Dally *et al.*, 1998 QTL mapping in testcrosses of flint lines of maize. III.

Comparison across populations for forage traits. Crop Sci. 38: 1278–1289.
McMullen, M. D., S. Kresovich, H. S. Villeda, P. Bradbury, H. Li *et al.*, 2009 Genetic properties of the maize nested association mapping population. Science 325: 737–740.
Méchin, V., O. Argillier, Y. Hebert, E. Guingo, L. Moreau *et al.*, 2001 Genetic analysis and QTL mapping of cell wall digestibility and lignification in silage maize. Crop Sci. 41: 690–697.
Meuwissen, T. H., and M. E. Goddard, 2001 Prediction of identity by descent probabilities from marker-haplotypes. Genet. Sel. Evol. 33: 605.
Meuwissen, T. H., B. J. Hayes, and M. E. Goddard, 2001 Prediction of total genetic value using genome-wide dense marker maps. Genetics 157: 1819–1829.
Peiffer, J. A., M. C. Romay, M. A. Gore, S. A. Flint-Garcia, Z. Zhang *et al.*, 2014 The genetic architecture of maize height. Genetics 196: 1337-1356.
Poland, J. A., P. J. Bradbury, E. S. Buckler, and R. J. Nelson, 2011 Genome-wide nested association mapping of quantitative resistance to northern leaf blight in maize. Proc. Natl. Acad. Sci. USA 108: 6893–6898.
R Core Team, 2013 *R: A Language and Environment for Statistical Computing*. R Foundation for Statistical Computing, Vienna, Austria.
Rebai, A., and B. Goffinet, 1993 Power of tests for QTL detection using replicated progenies derived from a diallel cross. Theor. Appl. Genet. 86: 1014–1022.
Rincent, R., L. Moreau, H. Monod, E. Kuhn, A. E. Melchinger *et al.*, 2014 Recovering power in association mapping panels with variable levels of linkage disequilibrium. Genetics 197: 375–387.
Romay, M. C., M. J. Millard, J. C. Glaubitz, J. A. Peiffer, K. L. Swarts *et al.*, 2013 Comprehensive genotyping of the USA national maize inbred seed bank. Genome Biol. 14: R55.
Salvi, S., G. Sponza, M. Morgante, D. Tomes, X. Niu *et al.*, 2007 Conserved noncoding genomic sequences associated with a flowering-time quantitative trait locus in maize. Proc. Natl. Acad. Sci. USA 104: 11376–11381.
Salvi, S., S. Castelletti, and R. Tuberosa, 2009 An updated consensus map for flowering time QTLs in maize. Maydica 54: 501–512.
Schön, C., B. Dhillon, H. Utz, and A. Melchinger, 2010 High congruency of QTL positions for heterosis of grain yield in three crosses of maize. Theor. Appl. Genet. 120: 321–332.
Segura, V., B. J. Vilhjálmsson, A. Platt, A. Korte, . Seren *et al.*, 2012 An efficient multi-locus mixed-model approach for genome-wide association studies in structured populations. Nat. Genet. 44: 825–830.
Sosnowski, O., A. Charcosset, and J. Joets, 2012 BioMercator V3: an upgrade of genetic map compilation and quantitative trait loci meta-analysis algorithms. Bioinformatics 28: 2082–2083.
Springer, N. M., K. Ying, Y. Fu, C. T. Yeh, Y. Jia *et al.*, 2009 Maize inbreds exhibit high levels of copy number variation (CNV) and presence/absence variation (PAV) in genome content. PLoS Genet. 11: e1000734.
Swanson-Wagner, R. A., S. R. Eichten, S. Kumari, P. Tiffin, J. C. Stein *et al.*, 2010 Pervasive gene content variation and copy number variation in maize and its undomesticated progenitor. Genome Res. 20: 1689–1699.
Tenaillon, M. I., and A. Charcosset, 2011 A European perspective on maize history. C. R. Biol. 334: 221–228.
Tian, F., P. J. Bradbury, P. J. Brown, H. Hung, Q. Sun *et al.*, 2011 Genome-wide association study of leaf architecture in the maize nested association mapping population. Nat. Genet. 43: 159–162.
van Inghelandt, D., J. C. Reif, B. S. Dhillon, P. Flament, and A. E. Melchinger, 2011 Extent and genome-wide distribution of linkage disequilibrium in commercial maize germplasm. Theor. Appl. Genet. 123: 11–20.
Würschum, T., W. Liu, M. Gowda, H. P. Maurer, S. Fischer *et al.*, 2012 Comparison of biometrical models for joint linkage association mapping. Heredity 108: 332–340.
Yu, J., G. Pressoir, W. H. Briggs, I. Vroh Bi, M. Yamasaki *et al.*, 2006 A unified mixed-model method for association mapping that accounts for multiple levels of relatedness. Nat. Genet. 38: 203–208.
Yu, J., J. B. Holland, M. D. McMullen, and E. S. Buckler, 2008 Genetic design and statistical power of nested association mapping in maize. Genetics 178: 539–551.

Communicating editor: B. S. Yandell

GENETICS

Supporting Information
http://www.genetics.org/lookup/suppl/doi:10.1534/genetics.114.169367/-/DC1

Linkage Disequilibrium with Linkage Analysis of Multiline Crosses Reveals Different Multiallelic QTL for Hybrid Performance in the Flint and Dent Heterotic Groups of Maize

Héloïse Giraud, Christina Lehermeier, Eva Bauer, Matthieu Falque, Vincent Segura, Cyril Bauland, Christian Camisan, Laura Campo, Nina Meyer, Nicolas Ranc, Wolfgang Schipprack, Pascal Flament, Albrecht E. Melchinger, Monica Menz, Jesús Moreno-González, Milena Ouzunova, Alain Charcosset, Chris-Carolin Schön, and Laurence Moreau

DOI: 10.1534/genetics.114.169367

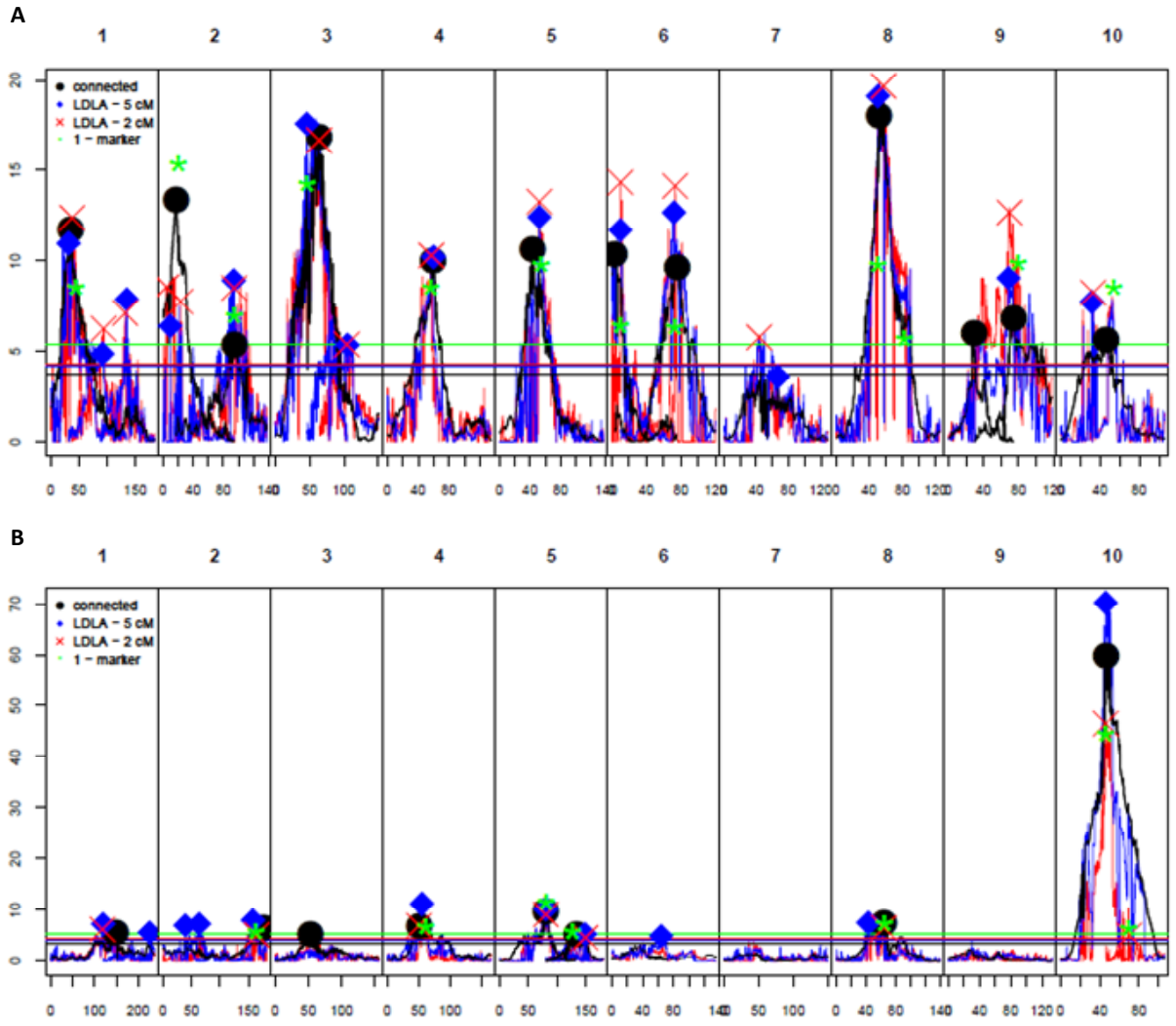

Figure S1 Results of the QTL detection with each model for DMC for **(A)** the dent design and **(B)** the flint design. The -log10(p-values) of the connected model are represented by black lines, the QTL positions of the connected models by black dots. The -log10(p-values) of the LDLA – 5 cM model are represented by blue lines and the QTL positions by blue diamonds. The -log10(p-values) of the LDLA – 2 cM model are represented by red lines and the QTL positions by red crosses. The -log10(p-values) of the QTL detected by the LDLA – 1-marker model are represented by green stars. Horizontal lines correspond to the threshold values of the different models.

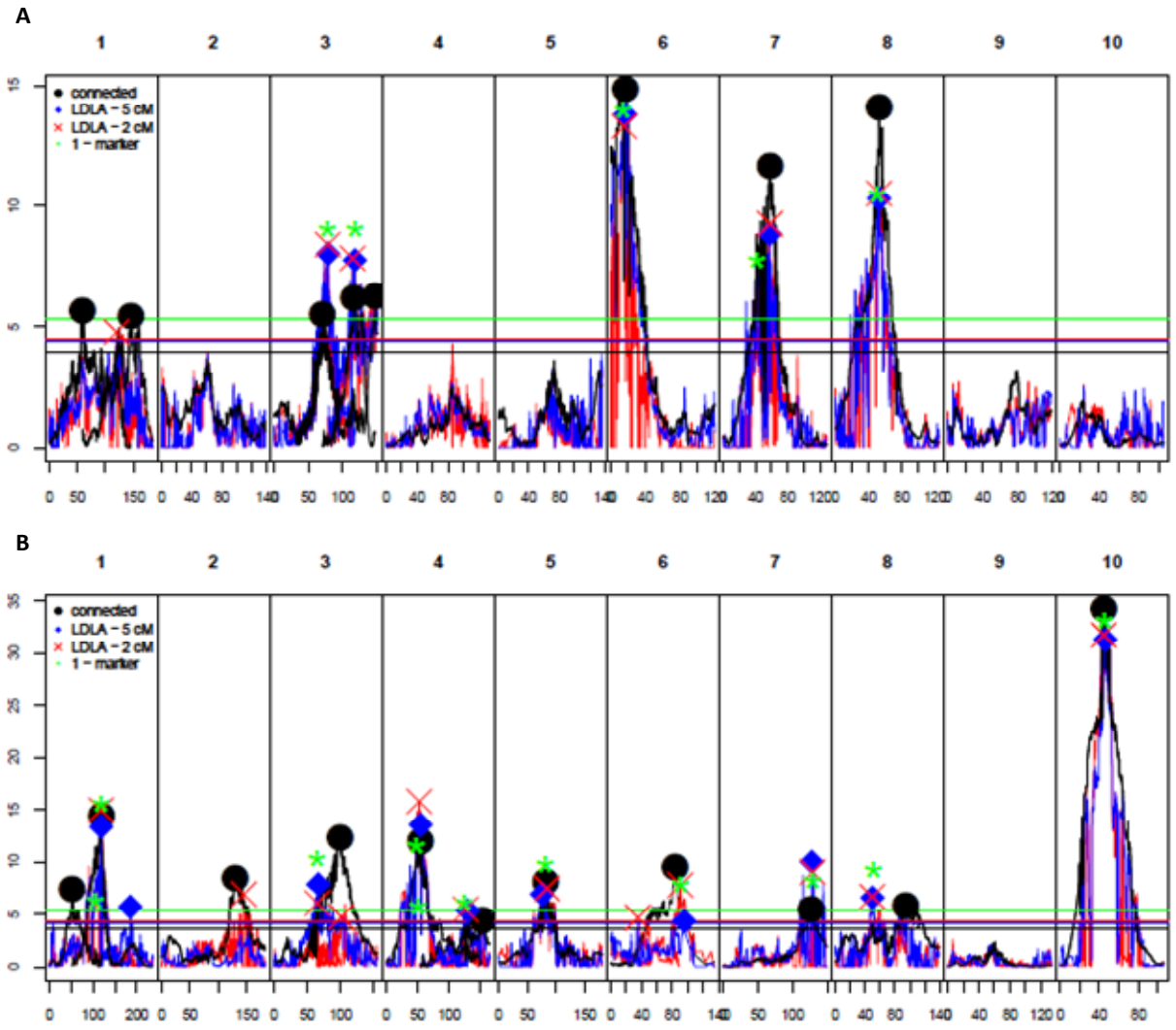

Figure S2 Results of the QTL detection with each model for DMY for **(A)** the dent design and **(B) the** flint design. The results for the dent design are in the superior part, flint in the inferior part. The -log10(p-values) of the connected model are represented by black lines, the QTL positions of the connected models by black dots. The - log10(p-values) of the LDLA – 5 cM model are represented by blue lines and the QTL positions by blue diamonds. The - log10(p-values) of the LDLA – 2 cM model are represented by red lines and the QTL positions by red crosses. The - log10(p-values) of the QTL detected by the LDLA – 1-marker model are represented by green stars. Horizontal lines correspond to the threshold values of the different models.

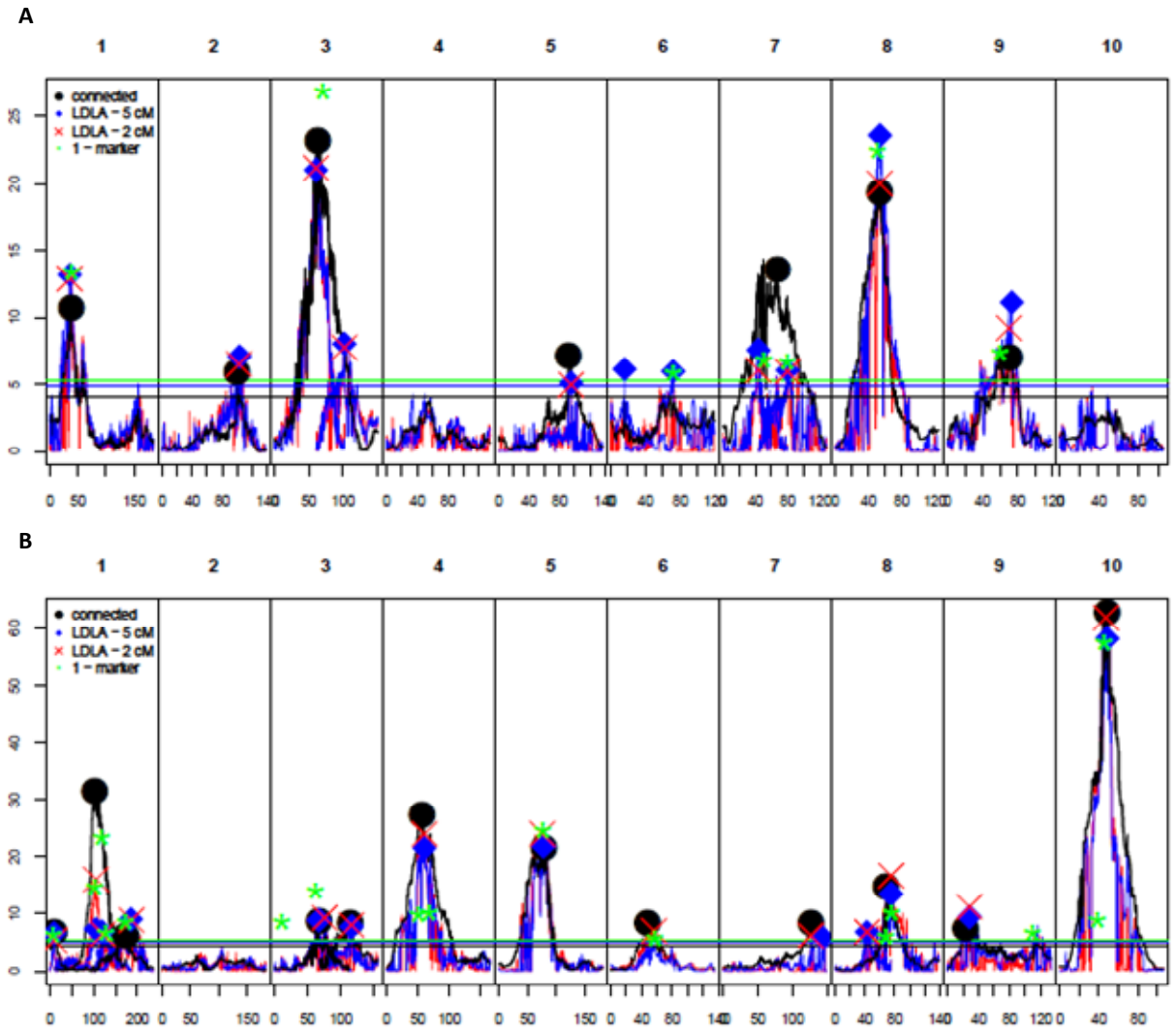

Figure S3 Results of the QTL detection with each model for DtTAS for **(A)** the dent design and **(B) the** flint design. The -log10(p-values) of the connected model are represented by black lines, the QTL positions of the connected models by black dots. The -log10(p-values) of the LDLA – 5 cM model are represented by blue lines and the QTL positions by blue diamonds. The -log10(p-values) of the LDLA – 2 cM model are represented by red lines and the QTL positions by red crosses. The -log10(p-values) of the QTL detected by the LDLA – 1-marker model are represented by green stars. Horizontal lines correspond to the threshold values of the different models.

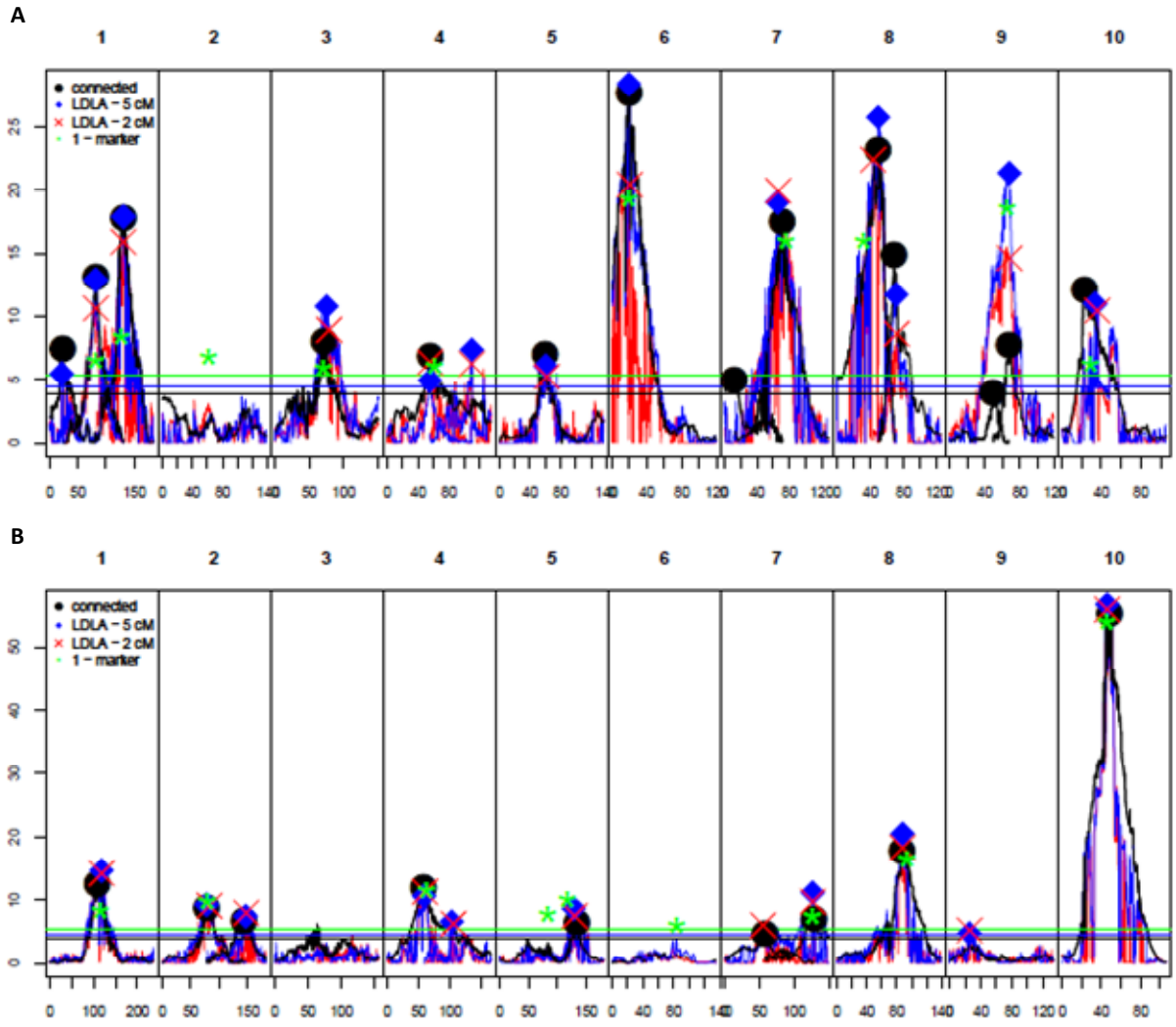

Figure S4 Results of the QTL detection with each model for PH for **(A)** the dent design and **(B) the** flint design. The -log10(p-values) of the connected model are represented by black lines, the QTL positions of the connected models by black dots. The -log10(p-values) of the LDLA – 5 cM model are represented by blue lines and the QTL positions by blue diamonds. The -log10(p-values) of the LDLA – 2 cM model are represented by red lines and the QTL positions by red crosses. The -log10(p-values) of the QTL detected by the LDLA – 1-marker model are represented by green stars. Horizontal lines correspond to the threshold values of the different models.

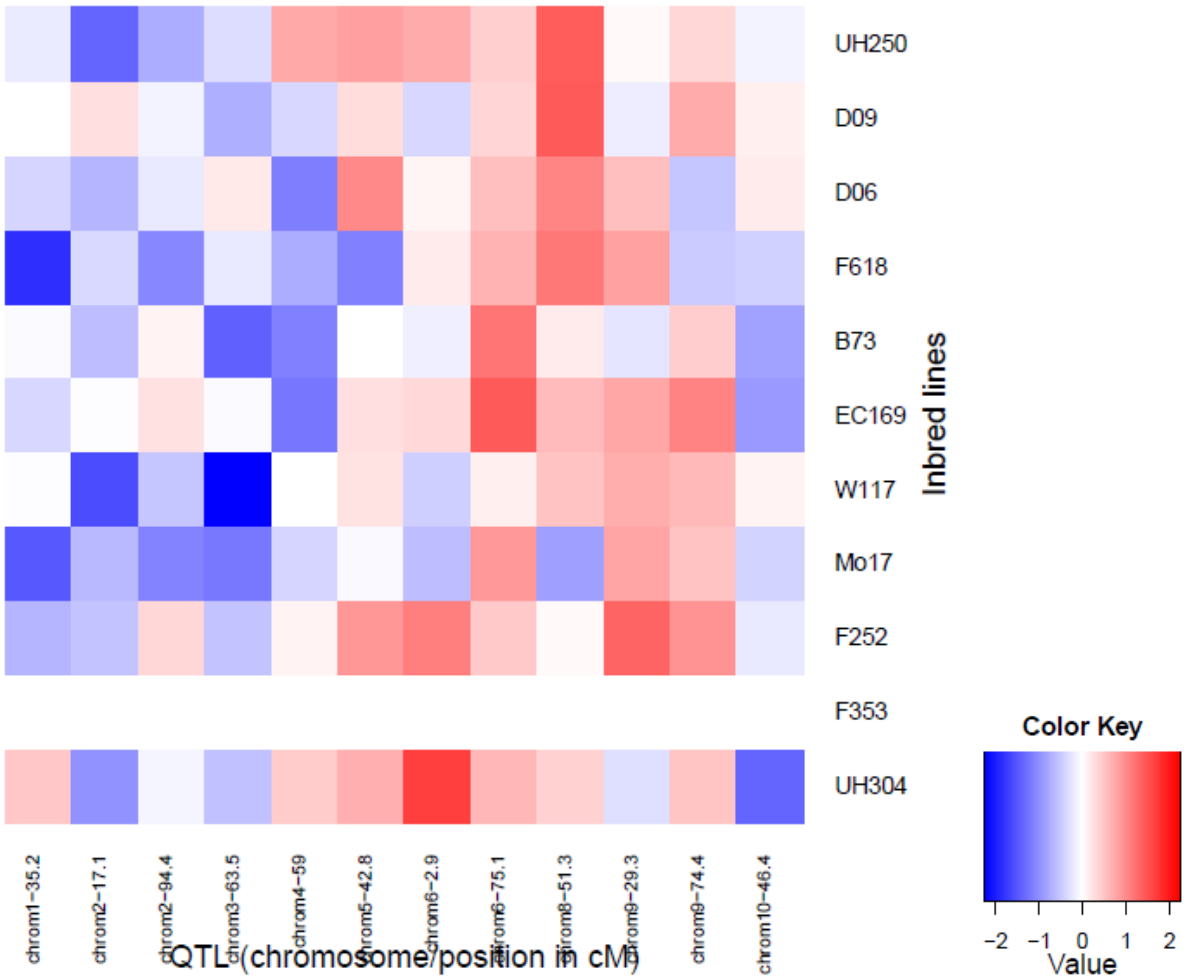

Figure S5 Allelic effects for the different dent lines for the QTL detected for DMC with the connected model. Allelic effects are estimated in contrast to the central line allelic effect (F353), which was set to zero.

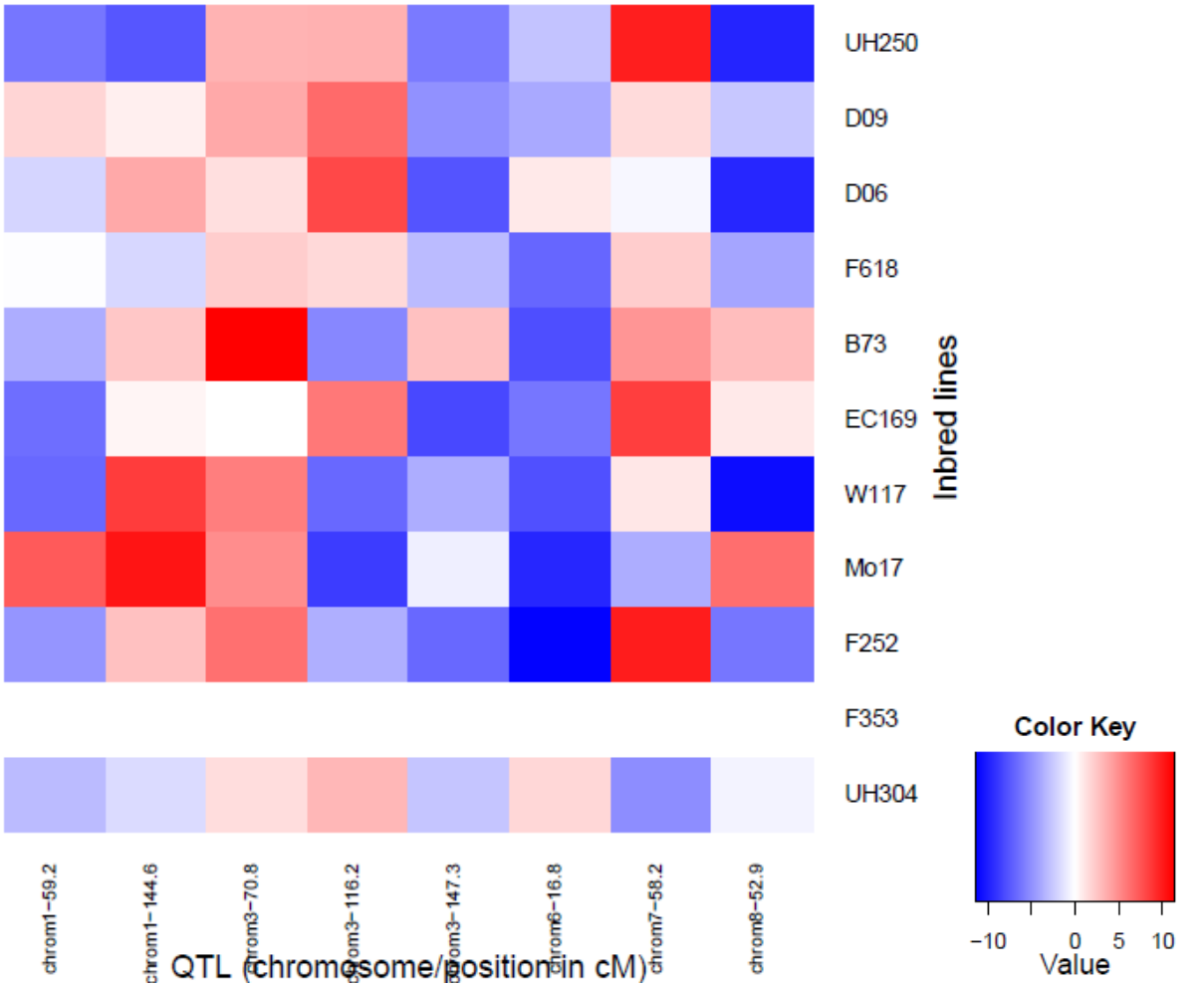

Figure S6 Allelic effects for the different dent lines for the QTL detected for DMY with the connected model. Allelic effects are estimated in contrast to the central line allelic effect (F353), which was set to zero.

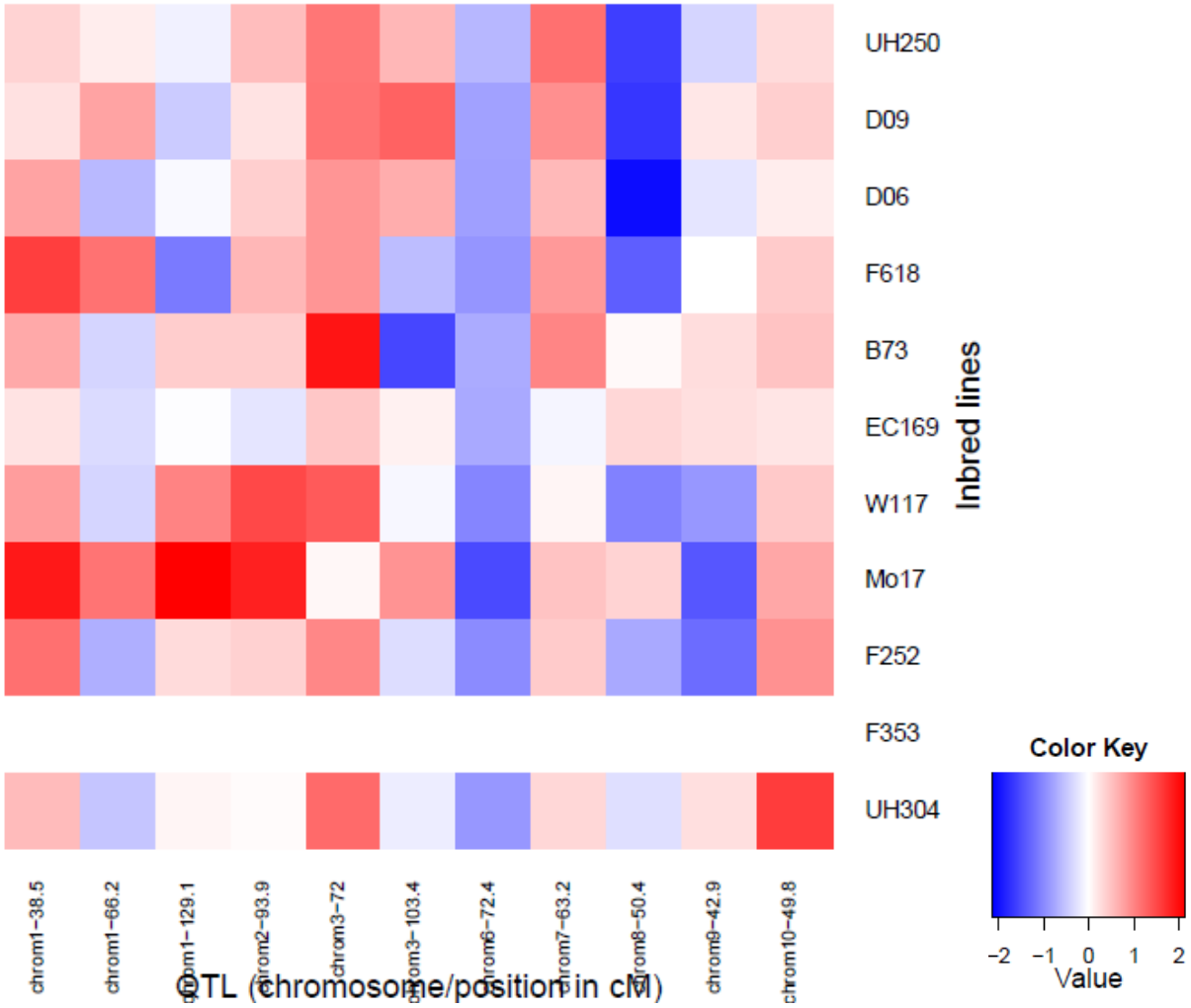

Figure S7 Allelic effects for the different dent lines for the QTL detected for DtSILK with the connected model. Allelic effects are estimated in contrast to the central line allelic effect (F353), which was set to zero.

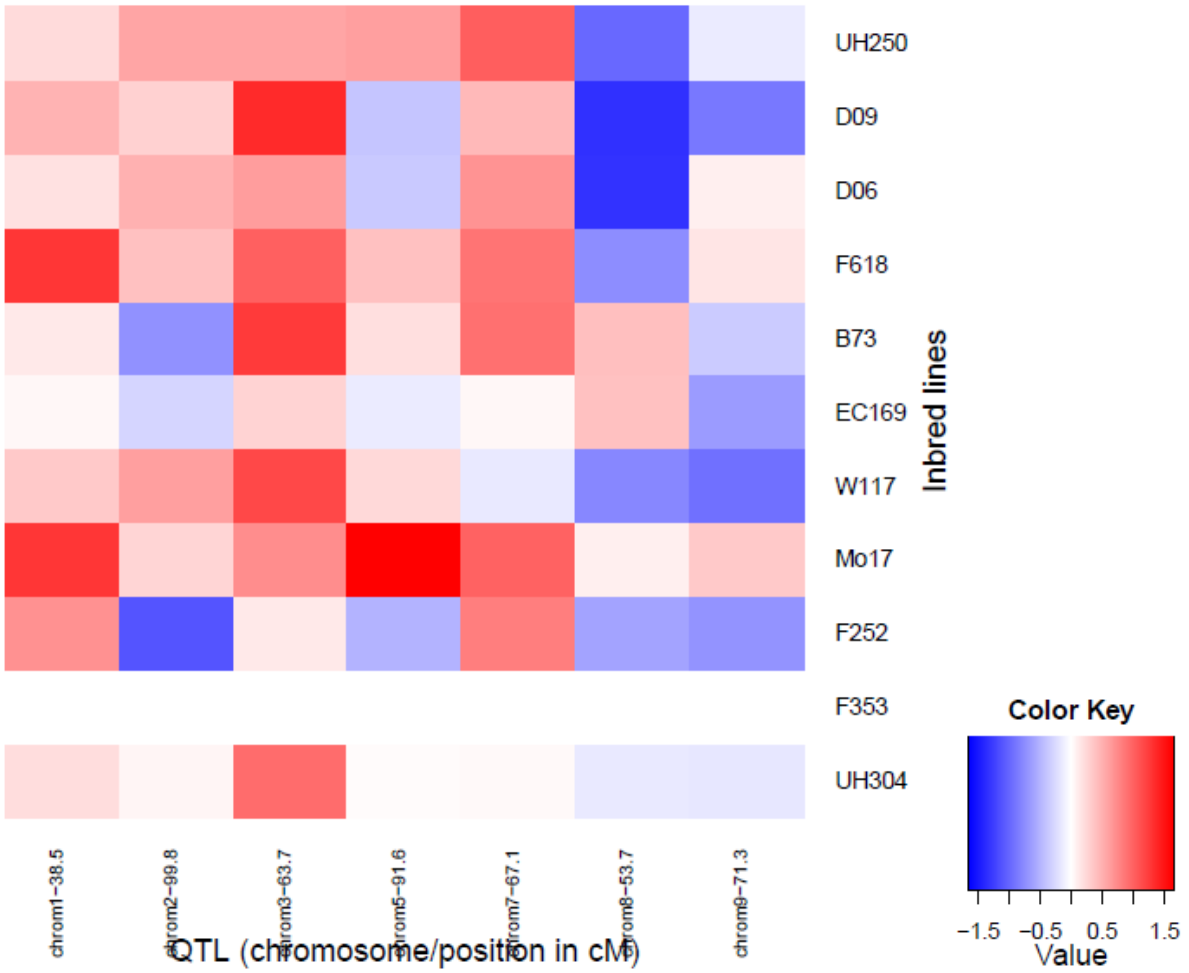

Figure S8 Allelic effects for the different dent lines for the QTL detected for DtTAS with the connected model. Allelic effects are estimated in contrast to the central line allelic effect (F353), which was set to zero.

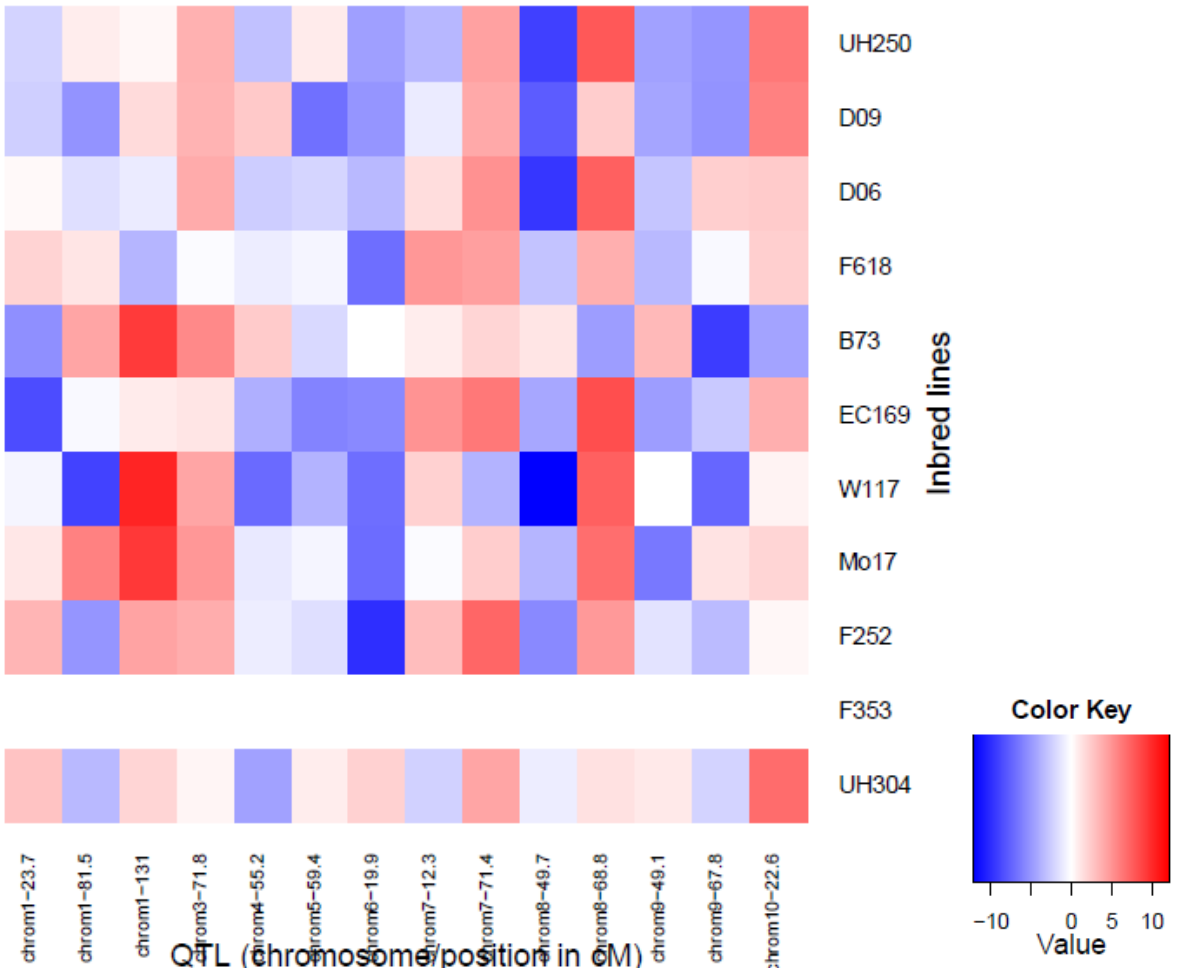

Figure S9 Allelic effects for the different dent lines for the QTL detected for PH with the connected model. Allelic effects are estimated in contrast to the central line allelic effect (F353), which was set to zero.

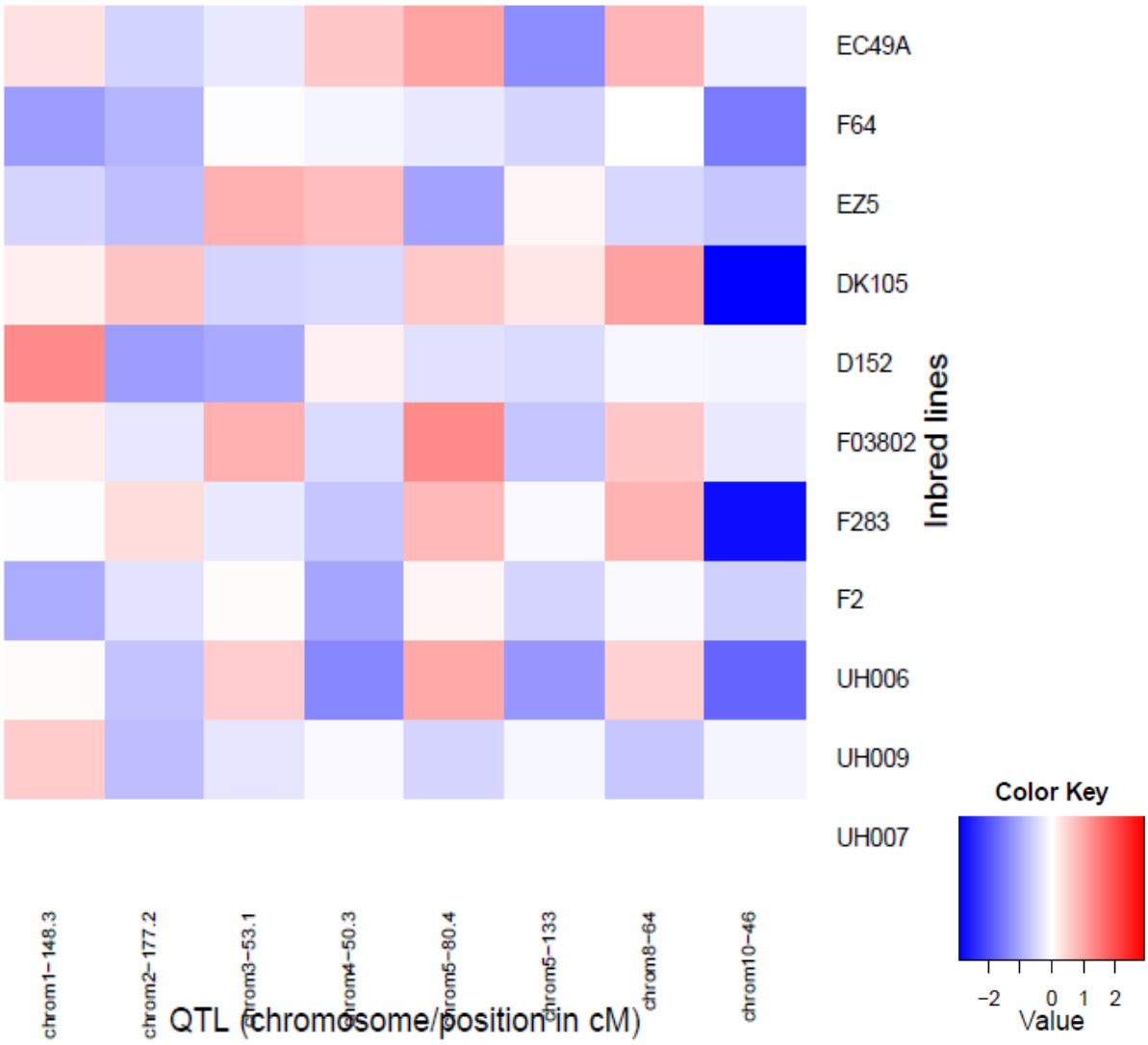

Figure S10 Allelic effects for the different flint lines for the QTL detected for DMC with the connected model. Allelic effects are estimated in contrast to the central line allelic effect (F353), which was set to zero. Allelic effects estimated for EP44 were not shown because the population where it segregates was too small (17 individuals) to obtain a reliable estimation.

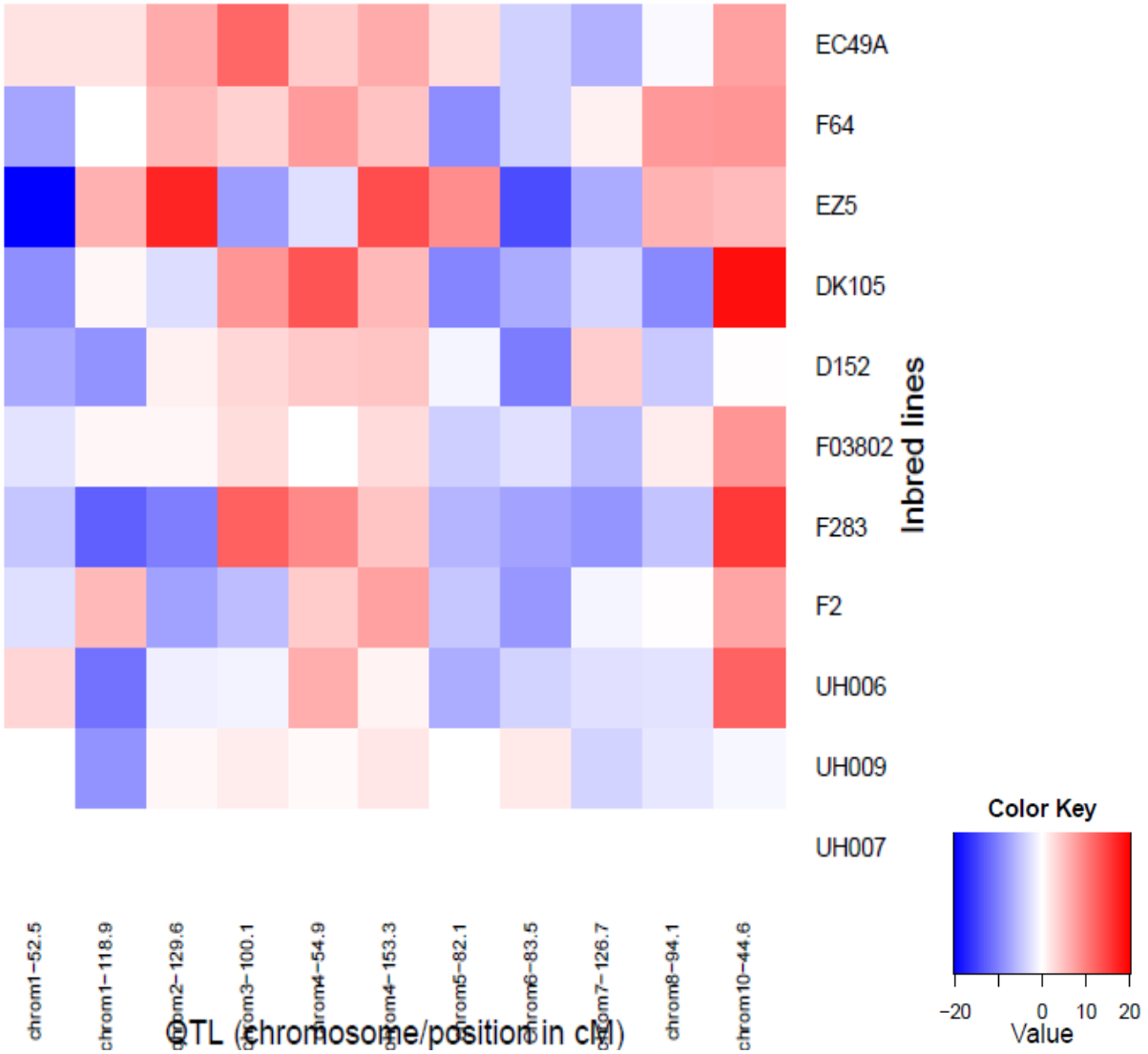

Figure S11 Allelic effects for the different flint lines for the QTL detected for DMY with the connected model. Allelic effects are estimated in contrast to the central line allelic effect (F353), which was set to zero. Allelic effects estimated for EP44 were not shown because the population where it segregates was too small (17 individuals) to obtain a reliable estimation.

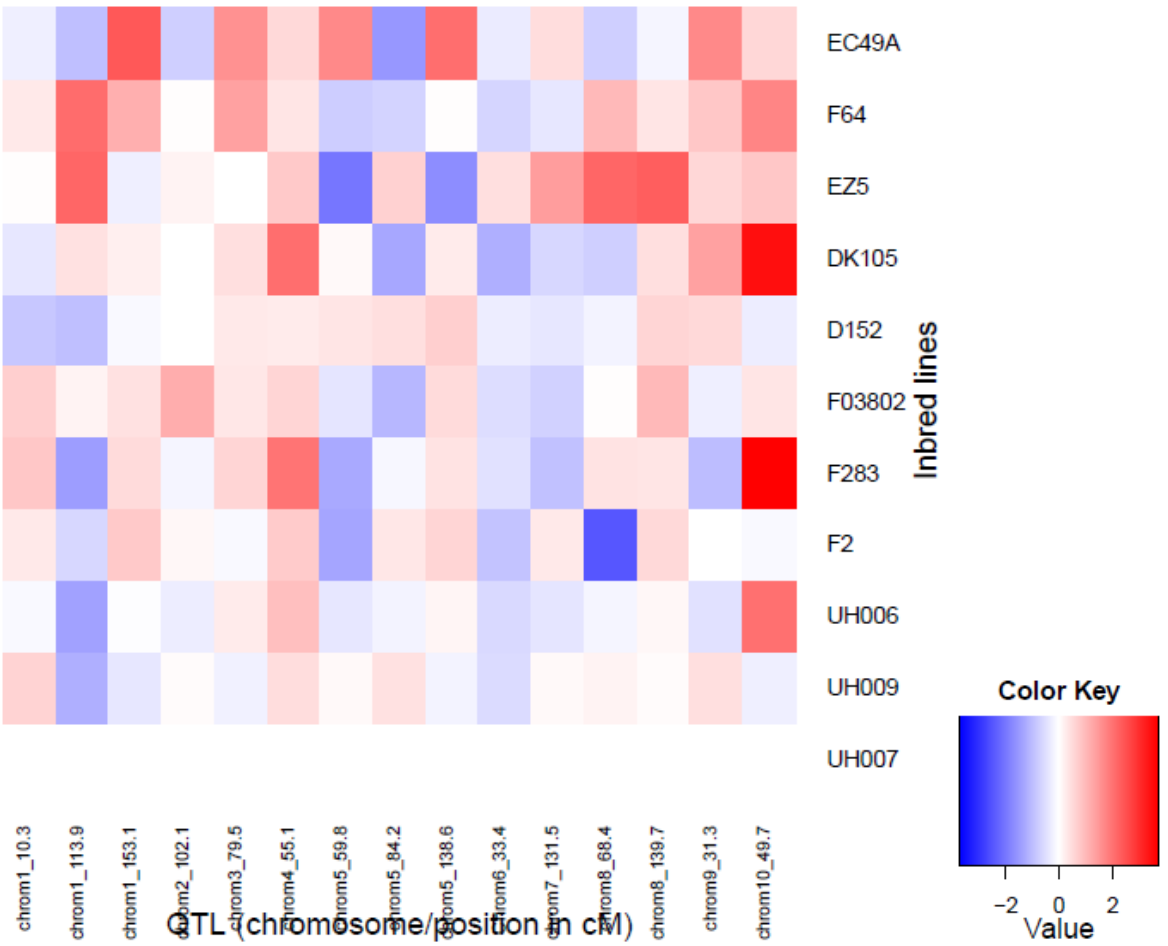

Figure S12 Allelic effects for the different flint lines for the QTL detected for DtSILK with the connected model. Allelic effects are estimated in contrast to the central line allelic effect (F353), which was set to zero. Allelic effects estimated for EP44 were not shown because the population where it segregates was too small (17 individuals) to obtain a reliable estimation.

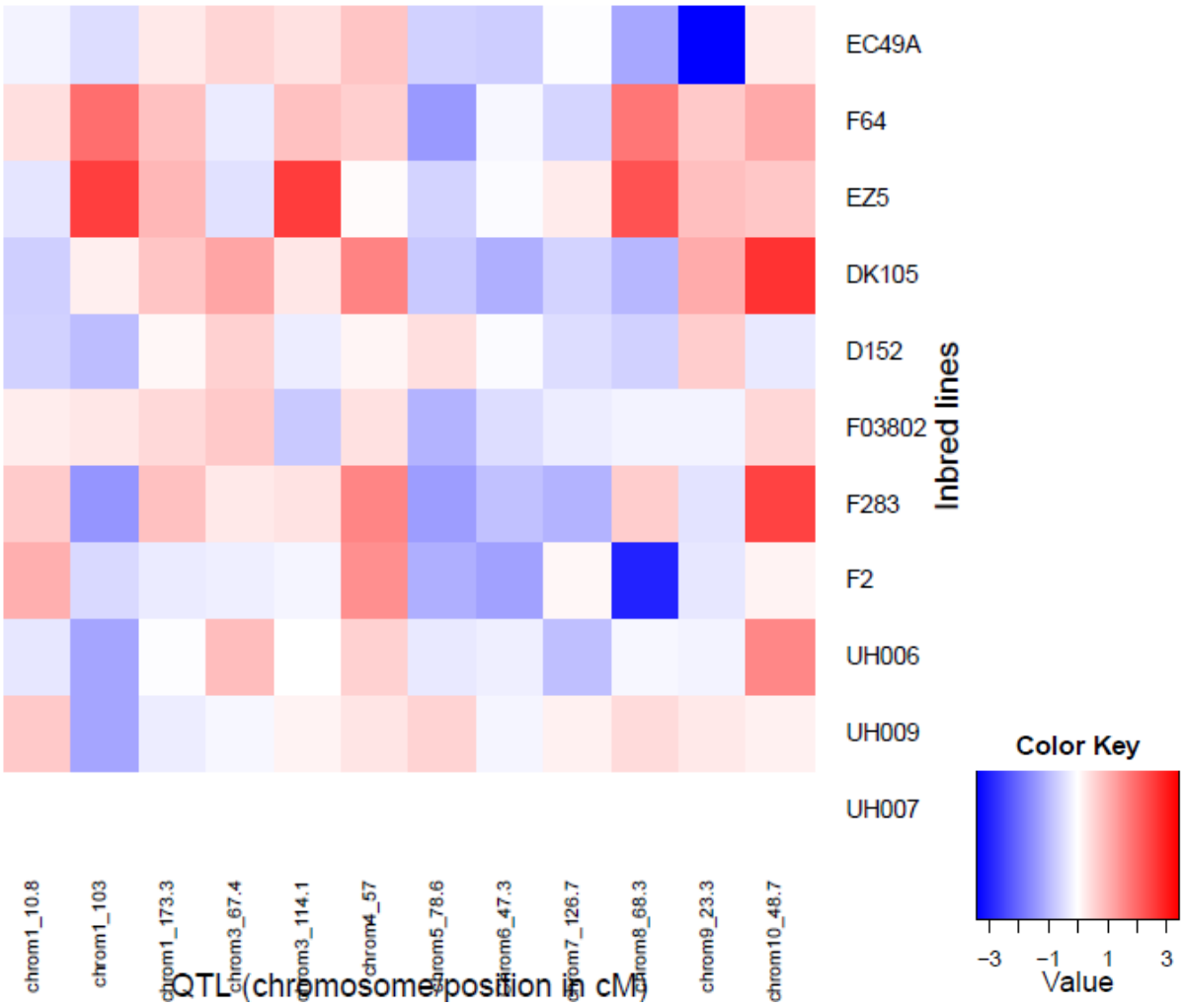

Figure S13 Allelic effects for the different flint lines for the QTL detected for DtTAS with the connected model. Allelic effects are estimated in contrast to the central line allelic effect (F353), which was set to zero. Allelic effects estimated for EP44 were not shown because the population where it segregates was too small (17 individuals) to obtain a reliable estimation.

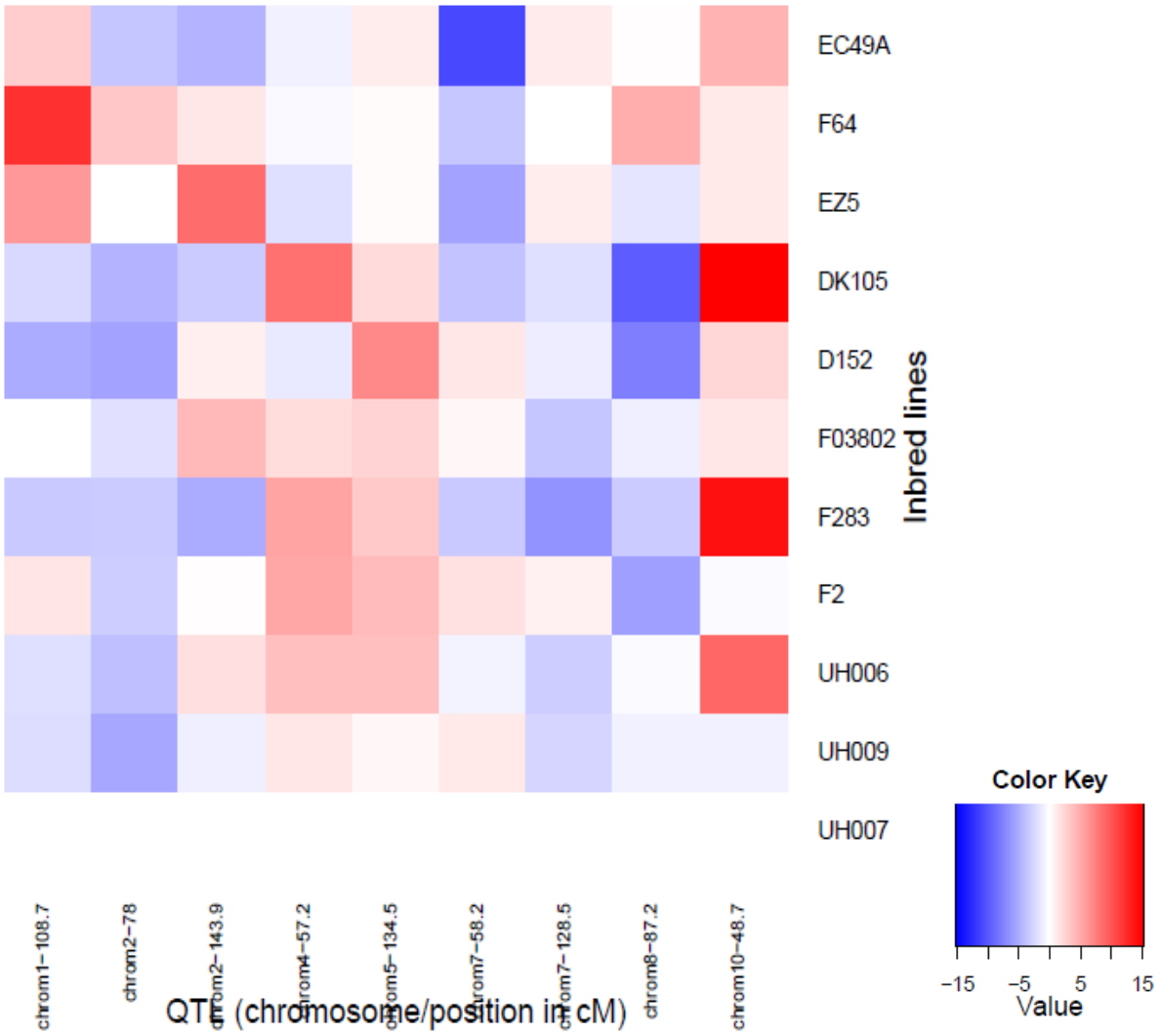

Figure S14 Allelic effects for the different flint lines for the QTL detected for PH with the connected model. Allelic effects are estimated in contrast to the central line allelic effect (F353), which was set to zero. Allelic effects estimated for EP44 were not shown because the population where it segregates was too small (17 individuals) to obtain a reliable estimation.

Table S1 Composition of the dent and flint designs with the number of DH lines in each family which were used for obtaining the consensus maps and the one which were phenotyped.

Dent design			**Flint design**		
Central line F353			Central line UH007		
Founder	Genotyped lines	Phenotyped lines	Founder	Genotyped lines	Phenotyped lines
B73	73	64	D152	112	72
D06	103	99	EC49A	53	29
D09	105	100	EP44	34[a]	17
EC169	77	66	EZ5	50	26
F252	105	96	F03802	129	129
F618	108	104	F2	77	54
Mo17	63	53	F283	134	133
UH250	99	94	F64	108	64
UH304	86	81	UH006	114	94
W117	100	84	UH009	117	98
			DK105	115	95
Total	**919**	**841**	**Total**	**1009**	**811**

[a] Population not used for mapping as too small

Table S2 Threshold values for the –log(p-value) for all the models and traits for the dent and flint groups and for the joint connected study.

	DMC	DMY	DtSILK	DtTAS	PH	**Mean**
Dent						
Connected	3.71	3.91	3.88	4.11	3.83	**3.89**
LDLA - 5cM	4.18	4.38	4.62	4.87	4.42	**4.49**
LDLA - 2cM	4.26	4.46	4.61	4.94	4.50	**4.55**
LDLA – 1-marker [a]	5.64	5.64	5.64	5.64	5.64	**5.64**
Flint						
Connected	3.43	3.65	4.15	4.37	3.83	**3.89**
LDLA - 5cM	4.07	4.20	4.84	5.13	4.53	**4.55**
LDLA - 2cM	4.30	4.36	5.04	5.23	4.60	**4.71**
LDLA – 1-marker [a]	5.61	5.61	5.61	5.61	5.61	**5.61**
Joint						
Connected	3.49	3.94	4.02	4.85	3.74	**4.00**

[a] The threshold value for the LDLA – 1-marker corresponded to a Bonferroni threshold for a genome-wide risk of 10 %. The other thresholds were calculated using 5,000 intra-family permutations of the phenotypes for a type I risk of 10 % across all families and the total genome.

Table S3 Results of the QTL detection in the flint design using the connected model. For each detected QTL, we showed its genetic position on the flint consensus map, its confidence interval, its level of significance and the partial percentage of variance explained. We also showed the name of one of the markers located at the detected position and their range of physical position(s) on the B73 v2 genome (Gore et al. 2009).

Trait	Nb	Chr	Marker	Physical position (kb)	Genetic position (cM)	Confidence interval	-log10(p)	R^2 (%)
DMC (%)	1	1	PZE_101172677	216581	148.3	142-149	5.4	3.2
	2	2	PZE_102191415	234096	177.2	176-181	6.6	3.6
	3	3	PZE_103033917	26445 - 138643	53.1	53-58	5.1	3
	4	4	PZE_104021549	18916 - 23142	50.3	49-55	6.7	3.7
	5	5	PZE_105085637	107137 - 138073	80.4	79-84	9.8	4.9
	6	5	PZE_105150268	201762	133	129-138	5.3	3.1
	7	8	PZE_108060399	107884 - 113068	64	50-65	7.4	4
	8	10	PZE_110049849	93025 - 115573	46	46-49	59.6	26.5
DMY (dt.ha-1)	1	1	PZE_101038989	25879 - 26917	52.5	52-54	7.4	3.8
	2	1	PZE_101147651	191513	118.9	117-120	14.4	6.4
	3	2	PZE_102152279	198891	129.6	127-141	8.5	4.2
	4	3	PZE_103137887	191279 - 196563	100.1	96-101	12.4	5.7
	5	4	PZE_104021283	22836	54.9	54-57	12.1	5.6
	6	4	PZE_104152609	237454 - 237702	153.3	127-154	4.5	2.7
	7	5	PZE_105078335	88752 - 139163	82.1	81-85	8.1	4.1
	8	6	PZE_106097864	151579	83.5	82-84	9.5	4.6
	9	7	PZE_107127708	170248	126.7	123-131	5.5	3.1
	10	8	PZE_108105216	159953	94.1	92-111	6	3.2
	11	10	PZE_110047350	88553 - 97551	44.6	44-45	34.2	14.2
DtSILK (d)	1	1	PZE_101005818	4452	10.3	9-12	6.9	2.2
	2	1	PZE_101143233	184616	113.9	101-115	26.3	6.7
	3	1	PZE_101181658	226175	153.1	148 -198	4.6	1.6
	4	2	PZE_102129781	178613 - 179981	102.1	101-162	5.4	1.8
	5	3	PZE_103121610	69965 - 179545	79.5	61-80	6.8	2.1
	6	4	PZE_104027603	23555 - 38027	55.1	52-57	31.8	8
	7	5	PZE_105033399	17477 - 18623	59.8	54-60	6.7	2.1
	8	5	PZE_105093579	135624 - 150088	84.2	80-86	7.3	2.2
	9	5	PZE_105163109	204822 - 205566	138.6	132-140	5.3	1.8
	10	6	PZE_106049962	99771	33.4	27-42	8	2.4
	11	7	PZE_107130719	171824	131.5	125-133	5.6	1.9
	12	8	PZE_108067425	119151	68.4	65-91	5.3	1.8
	13	8	PZE_108135936	175699 - 175734	139.7	117-140	6.1	2
	14	9	PZE_109009942	11080 - 11080	31.3	31-32	13	3.5

	15	10	PZE_110049100	91959 - 127347	49.7	49-50	94.6	27.5
DtTAS (d)	1	1	PZE_101005766	4609	10.8	9-13	6.8	2.5
	2	1	PZE_101108474	115220 - 161708	103	100-103	31.7	9
	3	1	PZE_101198020	246399 - 250557	173.3	164-175	6.2	2.3
	4	3	PZE_103098655	158895	67.4	67-68	9	3
	5	3	PZE_103153521	206703	114.1	110-115	8.5	2.9
	6	4	PZE_104025625	30431 - 37023	57	52-57	27.6	7.9
	7	5	PZE_105068746	71898 - 87721	78.6	78-79	21.6	6.3
	8	6	PZE_106061581	111966 - 112514	47.3	46-49	8.5	2.9
	9	7	PZE_107127708	170248	126.7	124-130	8.5	2.9
	10	8	PZE_108066752	118422 - 119082	68.3	68-69	15	4.6
	11	9	PZE_109007521	8233	23.3	23-38	7.6	2.6
	12	10	PZE_110048157	90243 - 122268	48.7	46-49	62.7	18.6
PH (cm)	1	1	PZE_101127891	162428 - 178788	108.7	108-109	12.7	5.4
	2	2	PZE_102074552	39031 - 55241	78	18-85	9	4.1
	3	2	PZE_102169535	213168	143.9	140-145	6.9	3.3
	4	4	PZE_104022475	23556 - 24765	57.2	55-60	12	5.1
	5	5	PZE_105151348	202416	134.5	132-136	6.4	3.2
	6	7	PZE_107061937	118305	58.2	53-62	4.9	2.6
	7	7	PZE_107128331	170536	128.5	121-129	7.2	3.4
	8	8	PZE_108098736	155052	87.2	87-92	17.8	7.1
	9	10	PZE_110048157	90243 - 122268	48.7	46-49	55.4	21.7

Table S4 Results of the QTL detection in the flint design using the LDLA – 5 cM model. For each detected QTL, we showed its genetic position on the flint consensus map, its confidence interval, its level of significance and the partial percentage of variance explained. We also showed the name of one of the markers located at the detected position and their range of physical position(s) on the B73 v2 genome (Gore et al. 2009).

Trait	Nb	Chr	Marker	Physical position (kb)	Genetic position (cM)	-log10(p)	R^2 (%)
DMC (%)	1	1	PZE_101147104	190602	119.4	7.3	2.9
	2	1	PZE_101250881	295590	225.9	5.6	2.2
	3	2	PZE_102025627	11947	39.2	7	1.8
	4	2	PZE_102046822	24366	63.7	7.3	3.4
	5	2	PZE_102183284	225854	157.9	8	3
	6	4	PZE_104021283	22836	54.9	11.2	4.8
	7	5	PZE_105085637	107137 - 138073	80.4	10.2	4.3
	8	5	PZE_105165365	208891 - 209048	148.7	5.2	1.6
	9	6	PZE_106076029	131411 - 134098	64.2	4.9	2.3
	10	8	PZE_108018911	18447	43.1	7.5	2.9
	11	10	PZE_110049849	93025 - 115573	46	70.2	29.2
DMY ($dt.ha^{-1}$)	1	1	PZE_101147651	191513	118.9	13.3	5.7
	2	1	PZE_101213494	263732	185.2	5.7	2.6
	3	3	PZE_103098382	158668 - 159808	66.8	7.9	4.1
	4	4	PZE_104020618	21905	55	13.5	6.3
	5	4	PZE_104123129	200190	129.8	5.3	2.9
	6	5	PZE_105068572	71700 - 72614	75.9	6.9	3.7
	7	6	PZE_106107736	156986	95.6	4.3	1.2
	8	7	PZE_107128866	170819	127.8	10	3.5
	9	8	PZE_108029326	27221 - 66473	50.1	6.6	3.4
	10	10	PZE_110045930	86778 - 109582	46.3	31.3	14.3
DtSILK (d)	1	1	PZE_101005818	4452	10.3	5.2	1.2
	2	1	PZE_101146834	190143	119.1	34.3	8.1
	3	1	PZE_101199192	248322	171.8	15	3.9
	4	2	PZE_102179704	222468	154.6	10.1	2.4
	5	3	PZE_103098382	158668 - 159808	66.8	8.2	2.4
	6	3	PZE_103121610	69965 - 179545	79.5	7.8	2
	7	4	PZE_104062511	44504 - 124929	62.6	31.7	8.1
	8	5	PZE_105078445	86146 - 140781	80.7	18.6	4.7
	9	5	PZE_105153835	204326 - 205504	137.6	10.9	2.4
	10	7	PZE_107133704	173181	139.3	7.6	1.6
	11	8	PZE_108066557	118189	68.7	7.4	1.9
	12	8	PZE_108133033	173617	133.8	6.6	1.1
	13	9	PZE_109009936	11079	31.6	11.6	2.8

	14	10	PZE_110048157	90243 - 122268	48.7	98.7	29.1
DtTAS (d)	1	1	PZE_101005765	4609	10	6.5	1.8
	1	1	PZE_101109004	116312 - 158005	105.3	7.3	2.5
	2	1	PZE_101147104	190602	119.4	6.9	2.2
	3	1	PZE_101213102	263154	185.3	9	2.7
	4	3	PZE_103098655	158895	67.4	8.9	2.7
	5	3	PZE_103158635	210426	116.9	7.7	2.2
	6	4	PZE_104044703	33362 - 96313	60.7	21.6	6.8
	7	5	PZE_105066936	69125 - 83278	77.8	21.9	6.5
	8	7	PZE_107136925	174718	144.3	5.7	1.3
	9	8	PZE_108019174	18351	42.8	6.8	2
	10	8	PZE_108073574	128549 - 128753	75.2	13.4	3.9
	11	9	PZE_109009220	10008 - 10009	28.4	9.5	2.4
	12	10	PZE_110048157	90243 - 122268	48.7	58.1	18.3
	13	1	PZE_101005765	4609	10	6.5	1.8
PH (cm)	1	1	PZE_101146427	189406	118.5	14.7	5.2
	2	2	PZE_102074552	39031 - 55241	78	9.3	3.8
	3	2	PZE_102173058	216192	146.8	7.4	2.9
	4	4	PZE_104045760	68246 - 68323	58.7	10.6	4.4
	5	4	PZE_104103602	179801 - 180054	102.8	6.6	2.4
	6	5	PZE_105150122	201632	128.7	8.7	2.7
	7	7	PZE_107128144	170420 - 170496	126.6	11.2	3.2
	8	8	PZE_108092331	149305 - 155644	87.8	20.5	7.8
	9	9	PZE_109008703	9311	25.5	4.8	1.3
	10	10	PZE_110049849	93025 - 115573	46	56.8	21.7

TableS5 Results of the QTL detection in the flint design using the LDLA – 2 cM model. For each detected QTL, we showed its genetic position on the flint consensus map, its confidence interval, its level of significance and the partial percentage of variance explained. We also showed the name of one of the markers located at the detected position and their range of physical position(s) on the B73 v2 genome (Gore et al. 2009).

Trait	Nb	Chr	Marker	Physical position (kb)	Genetic position (cM)	-log10(p)	R^2 (%)
DMC (%)	1	1	PZE_101146598	189773	118	6.2	2.5
	2	2	PZE_102185359	229130 - 229288	165	5	1.7
	3	4	PZE_104018885	18916 - 23142	50.3	6.9	3.4
	4	5	PZE_105085637	107137 - 138073	80.4	9.1	4.6
	5	5	PZE_105163718	208374	149.2	4.5	1.9
	6	8	PZE_108063241	113068 - 113206	64.1	6.5	3.2
	7	10	PZE_110049849	93025 - 115573	46	46.5	20.8
	8	10	PZE_110089009	139036	69.9	5	1.4
DMY ($dt.ha^{-1}$)	1	1	PZE_101146427	189406	118.5	14.9	5.3
	2	2	PZE_102172077	215135	144.9	6.9	2.5
	3	3	PZE_103097999	157939	65.4	6	1.9
	4	3	PZE_103142979	198520 - 198581	101.6	4.7	2.5
	5	4	PZE_104023433	26403 - 26403	52.7	15.8	5.8
	6	4	PZE_104122410	199546 - 199546	126.5	5.4	2.6
	7	5	PZE_105092759	133339 - 159961	84.4	7.4	3.7
	8	6	PZE_106050624	100745 - 103709	35.4	4.6	2.2
	9	6	PZE_106103665	155178	90.5	7.8	3.4
	10	7	PZE_107128846	170819	128.9	9	2.9
	11	8	PZE_108027746	26074 - 29164	49.5	6.7	3.4
	12	10	PZE_110047350	88553 - 97551	44.6	31.7	13.4
DtSILK (d)	1	1	PZE_101005818	4452	10.3	5.6	1.4
	2	1	PZE_101147104	190602	119.4	33.6	9.2
	3	1	PZE_101199859	248854 - 249092	173.9	14.2	4.1
	4	2	PZE_102181292	222435 - 223721	156.5	6.3	1.6
	5	3	PZE_103118006	176570	78.5	10.9	3
	6	3	PZE_103167997	216529	126.6	9.2	1.9
	7	4	PZE_104044892	42641 - 134020	62.5	29.6	8.8
	8	5	PZE_105039522	24542	63.6	18	5.4
	9	8	PZE_108133033	173617	133.8	9.2	2.1
	10	9	PZE_109010021	11134	30.1	11.9	2.9
	11	10	PZE_110060375	114622 - 114653	48.6	89.7	29.6
DtTAS(d)	1	1	PZE_101005770	4610	10.5	5.3	1.5
	2	1	PZE_101109004	116312 - 158005	105.3	16	4.7
	3	1	PZE_101147248	190703	121.1	6.4	1.7
	4	1	PZE_101213479	263702 - 265655	186.8	8.9	2.3

	5	3	PZE_103109418	170117 - 171781	75.9	9.3	2.1
	6	3	PZE_103157683	209726	116.3	8	2.1
	7	4	PZE_104044703	33362 - 96313	60.7	24	7.2
	8	5	PZE_105063310	62822 - 82069	76	24	7.1
	9	6	PZE_106064975	117082 - 122646	56.3	6.9	2.2
	10	7	PZE_107128144	170420 - 170496	126.6	6.1	1.4
	11	8	PZE_108019174	18351	42.8	6.8	1.9
	12	8	PZE_108073574	128549 - 128753	75.2	16.7	4.5
	13	9	PZE_109009220	10008 - 10009	28.4	11.2	2.5
	14	10	PZE_110049001	89438 - 108230	47.2	61.8	18.8
PH (cm)	1	1	PZE_101144184	187342 - 187381	118.6	14.2	4.6
	2	2	PZE_102076936	51554 - 59013	83	9.1	3.7
	3	2	PZE_102175167	217650	147.7	8	2.7
	4	4	PZE_104028514	34558 - 80248	60.2	11.3	4.8
	5	4	PZE_104104676	180887	105.6	6.2	1.5
	6	5	PZE_105144284	198198	130.3	7.5	1.9
	7	7	PZE_107057864	111123 - 112763	55.4	6	2.2
	8	7	PZE_107128144	170420 - 170496	126.6	9.7	2.8
	9	8	PZE_108092331	149305 - 155644	87.8	18.3	6.6
	10	9	PZE_109008133	8741	25.8	5.2	1.5
	11	10	PZE_110049849	93025 - 115573	46	56	21.3

Table S6 Results of the QTL detection in the flint design using the LDLA – 1-marker model. For each detected QTL, we showed its genetic position on the flint consensus map, its confidence interval, its level of significance and the partial percentage of variance explained. We also showed the name of one of the markers located at the detected position and their range of physical position(s) on the B73 v2 genome (Gore et al. 2009).

Trait	Nb	Chr	Marker	Physical position (kb)	Genetic position (cM)	-log10(p)	R^2 (%)
DMC (%)	1	2	PZE_102185353	229130	164.2	5.7	1.7
	2	4	PZE_104033064	40693	60	6.7	2.1
	3	5	PZE_105079359	90584	80.6	11.5	3.9
	4	5	PZE_105143697	197846	126.4	5.7	1.7
	5	8	PZE_108063319	113212	63.6	7.2	2.3
	6	10	PZE_110050010	94199	45.9	44.3	18.0
	7	10	PZE_110086343	137505	68.9	6.3	1.9
DMY ($dt.ha^{-1}$)	1	1	PZE_101128881	164375	105.8	6.3	1.8
	2	1	PZE_101144216	187381	118.6	15.6	5.2
	3	3	PZE_103097999	157939	65.4	10.3	3.3
	4	4	PZE_104017088	17150	48.7	11.4	3.7
	5	4	PZE_104021665	23190	51.4	5.8	1.7
	6	4	PZE_104122007	198999	124	6.0	1.7
	7	5	PZE_105094114	137392	81.5	9.7	3.1
	8	6	PZE_106104239	155466	90.7	7.8	2.4
	9	7	PZE_107128846	170819	128.9	8.2	2.5
	10	8	PZE_108028156	29898	51.1	9.1	2.9
	11	10	PZE_110050010	94199	45.9	33.0	12.2
DtSILK (d)	1	1	PZE_101004387	3883	8.5	8.2	1.5
	2	1	PZE_101088198	79735	90.5	10.0	1.9
	3	1	PZE_101106156	109635	102.4	17.1	3.6
	4	1	PZE_101151084	194731	125.8	9.4	1.8
	5	1	PZE_101200614	249700	173.1	11.3	2.2
	6	3	PZE_103098779	158974	61.9	11.3	2.2
	7	4	PZE_104021514	23073	51	9.0	1.7
	8	4	PZE_104079162	153502	69	10.8	2.1
	9	4	PZE_104152590	237693	155.7	6.4	1.1
	10	5	PZE_105069912	74335	76.8	21.1	4.6
	11	5	PZE_105143119	197706	127.6	5.7	1.0
	12	7	PZE_107128331	170536	128.5	6.5	1.2
	13	8	PZE_108070056	122950	71	12.0	2.4
	14	9	PZE_109009591	10597	30.3	7.1	1.3
	15	10	PZE_110016138	16504	38.6	11.2	2.2
	16	10	PZE_110050010	94199	45.9	45.7	11.1
DtTAS(d)	1	1	PZE_101004387	3883	8.5	6.1	1.2

	2	1	PZE_101115961	138907	103.5	14.5	3.3
	3	1	PZE_101144216	187381	118.6	23.2	5.6
	4	1	PZE_101160171	202307	128	6.7	1.3
	5	1	PZE_101200614	249700	173.1	8.5	1.8
	6	3	PZE_103007349	4064	11.7	8.6	1.8
	7	3	PZE_103098779	158974	61.9	14.0	3.2
	8	4	PZE_104021514	23073	51	9.7	2.1
	9	4	PZE_104079162	153502	69	10.0	2.1
	10	5	PZE_105069912	74335	76.8	24.7	6.0
	11	6	PZE_106066817	119166	57.4	5.5	1.0
	12	8	PZE_108067255	118970	68.8	5.8	1.1
	13	8	PZE_108074213	129415	75.5	10.3	2.2
	14	9	PZE_109111133	151251	109.1	6.5	1.3
	15	10	PZE_110018448	22128	38.9	8.9	1.9
	16	10	PZE_110050010	94199	45.9	57.5	16.1
PH (cm)	1	1	PZE_101145493	188172	115.6	8.3	2.4
	2	2	PZE_102074558	55249	79.5	9.8	3.0
	3	4	PZE_104042538	60023	63.1	11.6	3.6
	4	5	PZE_105091638	129996	83.4	7.8	2.3
	5	5	PZE_105134752	195420	117.6	9.9	3.0
	6	6	PZE_106097959	151785	84.1	6.1	1.7
	7	7	PZE_107127637	170111	126.3	7.4	2.1
	8	8	PZE_108105216	159953	94.1	16.6	5.3
	9	10	PZE_110050010	94199	45.9	53.9	20.6

Table S7 Results of the QTL detection in the dent design using the connected model. For each detected QTL, we showed its genetic position on the dent consensus map, its confidence interval, its level of significance and the partial percentage of variance explained. We also showed the name of one of the markers located at the detected position and their range of physical position(s) on the B73 v2 genome (Gore et al. 2009).

Trait	Nb	Chr	Marker	Physical position (kb)	Genetic position (cM)	Confidence interval	-log10(p)	R^2 (%)
DMC (%)	1	1	PZE_101031077	19101	35.2	32-39	11.7	4.8
	2	2	PZE_102011868	5425	17.1	16-18	13.4	5.3
	3	2	PZE_102149235	195177 - 197936	94.4	88-100	5.4	2.6
	4	3	PZE_103091082	150173 - 165855	63.5	58-64	16.8	6.5
	5	4	PZE_104079076	153406	59	57-61	10	4.2
	6	5	PZE_105026024	13303 - 13313	42.8	42-45	10.6	4.4
	7	6	PZE_106002839	3588 - 3869	2.9	1-6	10.4	4.3
	8	6	PZE_106098045	151822	75.1	72-79	9.6	4.1
	9	8	PZE_108058161	103705 - 103897	51.3	51-58	18	6.9
	10	9	PZE_109009836	10943	29.3	27-30	6	2.8
	11	9	PZE_109096235	141951	74.4	70-76	6.8	3.1
	12	10	PZE_110048796	91481 - 107902	46.4	27-53	5.7	2.7
DMY (dt.ha-1)	1	1	PZE_101071870	54342	59.2	57-62	5.7	3.8
	2	1	PZE_101215677	266310 - 266369	144.6	123-160	5.5	3.7
	3	3	PZE_103108908	169730 - 172477	70.8	66-76	5.5	3.7
	4	3	PZE_103160673	211719 - 212707	116.2	115-129	6.2	4
	5	3	PZE_103185177	229665	147.3	146-148	6.3	4.1
	6	6	PZE_106038467	86549	16.8	9-20	14.9	8
	7	7	PZE_107066645	123598 - 126465	58.2	57-61	11.7	6.6
	8	8	PZE_108057442	102536 - 108663	52.9	52-53	14.2	7.7
DtSILK (d)	1	1	PZE_101033622	21685	38.5	32-39	11.6	4.7
	2	1	PZE_101081841	69289 - 70518	66.2	65-67	4.6	2.3
	3	1	PZE_101194503	241368 - 244469	129.1	128-133	6.6	3
	4	2	PZE_102148927	195747 - 196529	93.9	93-96	9.1	3.8
	5	3	PZE_103110415	170772 - 174828	72	65-72	15.9	6.1
	6	3	PZE_103147207	201536 - 202769	103.4	101-110	5.5	2.6
	7	6	PZE_106095147	150309	72.4	70-74	13	5.1
	8	7	PZE_107072681	129265	63.2	43-67	8.4	3.6
	9	8	PZE_108057885	103311	50.4	50-54	26.4	9.6
	10	9	PZE_109020361	18684 - 20598	42.9	38-45	5	2.5
	11	10	PZE_110057591	110540 - 120784	49.8	49-52	7.2	3.2
DtTAS (d)	1	1	PZE_101033622	21685	38.5	36-39	10.8	5.4
	2	2	PZE_102157405	204235	99.8	99-100	6	3.4

	3	3	PZE_103101981	162179 - 167076	63.7	61-65	23.2	10.4
	4	5	PZE_105144068	198031	91.6	91-96	7.3	3.9
	5	7	PZE_107076807	132075	67.1	48-68	13.7	6.5
	6	8	PZE_108058411	104281 - 104625	53.7	50-55	19.4	8.8
	7	9	PZE_109092637	139196 - 140154	71.3	56-74	7.1	3.9
PH (cm)	1	1	PZE_101018818	10905	23.7	21-24	7.5	3
	2	1	PZE_101133561	172881 - 172940	81.5	80-84	13.2	4.7
	3	1	PZE_101196829	245032 - 245219	131	127-133	17.9	6.1
	4	3	PZE_103110278	170548	71.8	69-73	8.1	3.2
	5	4	PZE_104073340	138154 - 144727	55.2	53-58	6.9	2.8
	6	5	PZE_105065019	66038 - 79496	59.4	58-60	7.1	2.9
	7	6	PZE_106040994	89408 - 91643	19.9	19-20	27.7	9.1
	8	7	PZE_107005418	3665 - 3667	12.3	2-16	5.1	2.2
	9	7	PZE_107080996	135892	71.4	71-72	17.6	6
	10	8	PZE_108056028	100939 - 102711	49.7	49-52	23.3	7.7
	11	8	PZE_108078317	130737 - 134065	68.8	68-69	14.9	5.2
	12	9	PZE_109025803	25986	49.1	48-50	4	1.9
	13	9	PZE_109086708	134570 - 135460	67.8	67-70	7.8	3.1
	14	10	PZE_110008028	6072	22.6	22-26	12.2	4.4

Table S8 Results of the QTL detection in the dent design using the LDLA – 5 cM model. For each detected QTL, we showed its genetic position on the dent consensus map, its confidence interval, its level of significance and the partial percentage of variance explained. We also showed the name of one of the markers located at the detected position and their range of physical position(s) on the B73 v2 genome (Gore et al. 2009).

Trait	Nb	Chr	Marker	Physical position (kb)	Genetic position (cM)	-log10(p)	R^2 (%)
DMC (%)	1	1	PZE_101028121	16789 - 17963	31.6	11	3.9
	2	1	PZE_101150204	193868 - 194764	92	4.9	2
	3	1	PZE_101202934	249700 - 251159	134.9	7.9	3.1
	4	2	PZE_102006385	3379	9.6	6.4	1.5
	5	2	PZE_102150016	196649	94	8.9	2.9
	6	3	PZE_103038564	33572 - 56014	46	17.6	6.4
	7	3	PZE_103151042	204999	105	5.4	2.3
	8	4	PZE_104081311	155805	59.6	10.2	4
	9	5	PZE_105047074	35783 - 36699	52.3	12.4	4.9
	10	6	PZE_106007445	18846 - 21466	9.9	11.7	4.3
	11	6	PZE_106096901	150891	71.7	12.7	4.6
	12	7	PZE_107040665	154074	66.8	3.6	1.7
	13	8	PZE_108057885	103311	50.4	19.1	6.1
	14	9	PZE_109089324	137410	68.6	9	3.5
	15	10	PZE_110012467	10879	31.8	7.7	2.2
DMY ($dt.ha^{-1}$)	1	3	PZE_103116584	175989	78.9	8	3.9
	2	3	PZE_103162977	213416	117.8	7.8	4.3
	3	6	PZE_106038467	86549	16.8	13.8	8.1
	4	7	PZE_107066645	123598 - 126465	58.2	8.8	5.6
	5	8	PZE_108057442	102536 - 108663	52.9	10.3	5.8
DtSILK (d)	1	1	PZE_101033622	21685	38.5	22.6	7.2
	2	1	PZE_101205734	251079 - 254464	136.4	6.7	2.4
	3	2	PZE_102152020	198672	94.5	15	4.5
	4	3	PZE_103086165	142732 - 157202	61.7	10	3.6
	5	3	PZE_103122617	180515	78.6	16.3	4.7
	6	5	PZE_105049624	41635 - 58706	56.3	4.8	2.2
	7	6	PZE_106094705	149930	71	16.5	5.4
	8	7	PZE_107045046	25471 - 104886	43.9	7.4	3
	9	7	PZE_107107125	158951 - 158952	82.1	5.8	2
	10	8	PZE_108058411	104281 - 104625	53.7	27.7	8.9
	11	9	PZE_109098496	143352	77.3	5.5	2
	12	10	PZE_110057591	110540 - 120784	49.8	8	3.1
DtTAS(d)	1	1	PZE_101032015	19641 - 21075	35.7	13.2	4.8
	2	2	PZE_102159907	206081 - 207151	102.9	7.1	2.8
	3	3	PZE_103098157	158352	60.8	21	7.6

	4	3	PZE_103143600	199245 - 201331	102.2	8	3.1
	5	5	PZE_105143985	197957 - 200116	95.6	5.1	2
	6	6	PZE_106033981	79499 - 86347	16	6.1	2.7
	7	6	PZE_106092387	148530 - 150461	72	6	2.5
	8	7	PZE_107045046	25471 - 104886	43.9	7.6	3.4
	9	7	PZE_107099124	152685 - 155704	79.9	6.1	2.7
	10	8	PZE_108062375	111291	54.3	23.6	8.3
	11	9	PZE_109094832	141175	73.4	11.1	3.9
PH (cm)	1	1	PZE_101018868	10962	21.4	5.5	2.1
	2	1	PZE_101133356	172811	81.4	12.9	4.4
	3	1	PZE_101196829	245032 - 245219	131	17.9	6.1
	4	3	PZE_103111112	171438 - 175550	75.5	10.8	3.9
	5	4	PZE_104073340	138154 - 144727	55.2	4.9	2
	6	4	PZE_104136077	202589 - 227111	109.7	7.4	2.6
	7	5	PZE_105068432	70082 - 86033	60.4	6.1	2.7
	8	6	PZE_106040975	89403 - 89404	19.3	28.4	9.3
	9	7	PZE_107076796	132076	65.4	19	6.3
	10	8	PZE_108056028	100939 - 102711	49.7	25.7	8.2
	11	8	PZE_108079422	133563 - 138524	71.4	11.7	4.1
	12	9	PZE_109085253	133933	68.1	21.3	7.2
	13	10	PZE_110014332	11179 - 13553	33.8	11	3.3

Table S9 Results of the QTL detection in the dent design using the LDLA – 2 cM model. For each detected QTL, we showed its genetic position on the dent consensus map, its confidence interval, its level of significance and the partial percentage of variance explained. We also showed the name of one of the markers located at the detected position and their range of physical position(s) on the B73 v2 genome (Gore et al. 2009).

Trait	Nb	Chr	Marker	Physical position (kb)	Genetic position (cM)	-log10(p)	R^2 (%)
DMC (%)	1	1	PZE_101036345	23712	38	12.4	4
	2	1	PZE_101154088	194939 - 197272	93.9	6.2	2.3
	3	1	PZE_101203104	250888	131.9	7.1	2.8
	4	2	PZE_102002360	1724	4.7	8.5	2
	5	2	PZE_102017964	8279	23.4	7.7	2.2
	6	2	PZE_102152020	198672	94.5	8.5	3
	7	3	PZE_103093079	154090 - 160936	63.9	16.7	5.4
	8	3	PZE_103148259	202185	104.1	5.4	2
	9	4	PZE_104076988	151510 - 151684	56.9	10.3	3.5
	10	5	PZE_105047074	35783 - 36699	52.3	13.3	4.9
	11	6	PZE_106020123	14400 - 24611	10	14.3	4.4
	12	6	PZE_106097959	151785	73.1	14.1	4.3
	13	7	PZE_107045895	24563 - 103626	43.6	5.8	2.4
	14	8	PZE_108061901	110744 - 115294	57.2	19.7	6.4
	15	9	PZE_109091148	138616 - 138617	69.6	12.7	4.2
	16	10	PZE_110012769	11241	33	8.2	2.2
DMY ($dt.ha^{-1}$)	1	1	PZE_101183895	228556	119.6	4.8	2.3
	2	3	PZE_103113115	172857 - 178134	78.3	8.4	4
	3	3	PZE_103159262	210755 - 210760	114.6	7.8	3.7
	4	6	PZE_106032535	75517 - 86627	15.5	13.3	6.9
	5	7	PZE_107069530	126351	58.1	9.3	5
	6	8	PZE_108057745	103023 - 103457	53	10.5	5.8
DtSILK (d)	1	1	PZE_101035008	19696 - 22646	37.8	22	6.9
	2	1	PZE_101205734	251079 - 254464	136.4	7.4	2.2
	3	2	PZE_102151348	197954	94.7	12.9	4.1
	4	3	PZE_103086165	142732 - 157202	61.7	10.2	3.7
	5	3	PZE_103122617	180515	78.6	16.3	4.7
	6	5	PZE_105049624	41635 - 58706	56.3	4.9	2.3
	7	6	PZE_106095370	150525 - 150588	72.6	17.5	5.1
	8	7	PZE_107045046	25471 - 104886	43.9	8.7	3.3
	9	7	PZE_107106025	158126	81.1	6.1	2
	10	8	PZE_108062521	111781	54.6	28.2	8.9
	11	9	PZE_109098632	143808	78.5	6.1	2.1
	12	10	PZE_110057591	110540 - 120784	49.8	7.8	3
DtTAS(d)	1	1	PZE_101032015	19641 - 21075	35.7	12.9	5

	2	2	PZE_102161022	207043	102.3	6.5	2.6
	3	3	PZE_103098157	158352	60.8	21.2	8.3
	4	3	PZE_103143600	199245 - 201331	102.2	7.8	3.2
	5	5	PZE_105143697	197846 - 200369	95.5	5	2.2
	6	7	PZE_107045046	25471 - 104886	43.9	6.1	2.9
	7	7	PZE_107099124	152685 - 155704	79.9	6	2.9
	8	8	PZE_108058411	104281 - 104625	53.7	20	7.6
	9	9	PZE_109090152	137787 - 138020	70.1	9.2	3.7
PH (cm)	1	1	PZE_101132703	171230 - 178401	82.3	10.6	4.1
	2	1	PZE_101196829	245032 - 245219	131	15.9	6
	3	3	PZE_103119393	178152 - 178564	79.1	8.9	2.8
	4	4	PZE_104073794	145614	55.7	6.4	2.5
	5	4	PZE_104138654	204861 - 226068	109.4	6.2	2.5
	6	5	PZE_105070660	74660 - 145496	61.9	5.2	2.5
	7	6	PZE_106044620	93734	20.4	20.4	6.4
	8	7	PZE_107077092	132190	66.5	19.9	6.5
	9	8	PZE_108038271	26346 - 65101	43.6	22.4	8.1
	10	8	PZE_108081297	133441 - 143002	71.9	8.6	3.3
	11	9	PZE_109085253	133933	68.1	14.6	5.4
	12	10	PZE_110013838	12922	35.9	10.4	4.2

Table S10 Results of the QTL detection in the dent design using the LDLA – 1-marker model. For each detected QTL, we showed its genetic position on the dent consensus map, its confidence interval, its level of significance and the partial percentage of variance explained. We also showed the name of one of the markers located at the detected position and their range of physical position(s) on the B73 v2 genome (Gore et al. 2009).

Trait	Nb	Chr	Marker	Physical position (kb)	Genetic position (cM)	-log10(p)	R^2 (%)
DMC (%)	1	1	PZE_101043094	29355	43.3	8.5	2.6
	2	2	PZE_102015152	6459	20.9	15.3	5.1
	3	2	PZE_102150016	196649	94	6.9	2.0
	4	3	PZE_103038375	33073	45.8	14.2	4.7
	5	4	PZE_104077580	151818	57	8.5	2.6
	6	5	PZE_105043990	31444	54.4	9.7	3.0
	7	6	PZE_106020569	16293	9.3	6.4	1.9
	8	6	PZE_106092387	148530	72	6.3	1.8
	9	8	PZE_108054499	97030	50.2	9.8	3.1
	10	8	PZE_108104357	159498	81.9	5.6	1.6
	11	9	PZE_109098884	143900	78.9	9.8	3.1
	12	10	PZE_110073412	130077	53.5	8.5	2.6
DMY ($dt.ha^{-1}$)	1	3	PZE_103115334	175353	78.1	9.0	3.6
	2	3	PZE_103162977	213416	117.8	9.0	3.7
	3	6	PZE_106031833	74460	14.6	14.0	6.0
	4	7	PZE_107026145	29198	41.6	7.7	3.0
	5	8	PZE_108054494	97029	50.5	10.4	4.3
DtSILK (d)	1	1	PZE_101032230	19696	37.8	8.8	2.4
	2	1	PZE_101076734	60701	61	11.4	3.3
	3	2	PZE_102150016	196649	94	8.9	2.5
	4	3	PZE_103104448	165863	71.3	15.7	4.7
	5	3	PZE_103132614	188530	91.1	8.1	2.2
	6	5	PZE_105054634	51432	55.4	6.4	1.7
	7	6	PZE_106092387	148530	72	13.8	4.1
	8	7	PZE_107023943	25471	43.9	13.0	3.8
	9	8	PZE_108026961	27634	45.5	5.7	1.5
	10	8	PZE_108063387	113292	57.3	10.1	2.9
	11	10	PZE_110062675	117753	50.1	6.9	1.8
DtTAS(d)	1	1	PZE_101035341	23055	39.2	13.3	4.6
	2	3	PZE_103104448	165863	71.3	26.8	10.1
	3	6	PZE_106092387	148530	72	5.8	1.8
	4	7	PZE_107061937	118305	50.8	6.8	2.1
	5	7	PZE_107100713	155251	79.6	6.7	2.1
	6	8	PZE_108057325	102454	51.5	22.5	8.3
	7	9	PZE_109071914	116752	59.8	7.3	2.3

PH (cm)	1	1	PZE_101132469	170852	80.9	6.5	1.9
	2	1	PZE_101191970	238427	127.1	8.4	2.6
	3	2	PZE_102068532	46438	61.8	6.8	2.0
	4	3	PZE_103104448	165863	71.3	6.0	1.7
	5	4	PZE_104082879	156995	61.4	6.0	1.7
	6	6	PZE_106040890	89137	19.4	19.4	6.7
	7	7	PZE_107084200	139526	76.4	15.9	5.4
	8	8	PZE_108014288	14088	32	15.9	5.4
	9	9	PZE_109080822	128851	65.9	18.5	6.4
	10	10	PZE_110009551	7563	29.4	6.3	1.8

Table S11 Results of the QTL detection in the joint analysis using the connected model. For each detected QTL, we showed its genetic position on the dent-flint consensus map, its confidence interval, its level of significance and the partial percentage of variance explained. We also showed the name of one of the markers located at the detected position and their range of physical position(s) on the B73 v2 genome (Gore et al. 2009).

Trait	Nb	Chr	Marker	Physical position (kb)	Genetic position (cM)	-log10(p)	R^2 (%)
DMC (%)	1	1	PZE_101032230	19696 - 19975	41.3	8.5	2.3
	2	1	PZE_101103995	104611 - 113689	93.3	5.2	1.7
	3	1	PZE_101202934	251103 - 251159	160.4	4.5	1.6
	4	1	PZE_101247063	292581	200.4	4.3	1.5
	5	2	PZE_102012595	5556	17.2	21.4	4.5
	6	2	PZE_102178263	220854	131.3	6.9	2
	7	3	PZE_103033638	26310 - 30050	45.4	9.3	2.5
	8	3	PZE_103100449	160755	65.5	7.5	2.1
	9	4	PZE_104032843	40344 - 65470	54.6	13.8	3.3
	10	4	PZE_104143137	231732	130.7	4.4	1.6
	11	5	PZE_105025123	12581	42.6	17.6	3.8
	12	6	PZE_106005094	6514	6.3	10.1	2.6
	13	6	PZE_106082658	139918 - 142454	66	11.8	2.9
	14	7	PZE_107012564	9201	33.9	4.7	1.6
	15	8	PZE_108063387	112547 - 113298	63.4	21.7	4.5
	16	9	PZE_109010670	11079 - 11504	30.8	3.9	1.5
	17	9	PZE_109096248	141983	82.5	5.4	1.7
	18	10	PZE_110047687	89209 - 111680	47.7	68.5	12.5
DMY (dt.ha-1)	1	1	PZE_101145302	188026 - 188087	109.4	12.2	3.6
	2	1	PZE_101215394	266047	170.9	10.4	3.2
	3	2	PZE_102013856	5997 - 6049	18.5	5.2	2.1
	4	2	PZE_102066516	44332	67.4	7.2	2.6
	5	3	PZE_103010658	5853	21.6	7.6	2.6
	6	3	PZE_103098655	158895 - 161562	65.7	9.5	3.1
	7	3	PZE_103162977	213416	120.4	5.3	2.1
	8	4	PZE_104025845	28986 - 32061	51.5	13.5	3.9
	9	5	PZE_105103128	155811 - 160460	78	8.8	2.9
	10	6	PZE_106037747	81440 - 86559	18.3	9.9	3.1
	11	6	PZE_106050075	99944	34	11.4	3.4
	12	6	PZE_106106971	156749	88.4	9.2	3
	13	7	PZE_107025551	28013 - 100690	44.8	8.3	2.8
	14	7	PZE_107127637	170111 - 170248	119.3	5.9	2.3
	15	8	PZE_108060398	107884 - 111781	62.1	12.1	3.6
	16	10	PZE_110043381	82670 - 84599	43.2	38.6	8.9
DtSILK (d)	1	1	PZE_101005770	4452 - 4610	9.4	6.4	1.8

	2	1	PZE_101034085	21984 - 21992	42.7	10	2.3
	3	1	PZE_101105390	102985 - 118116	93.6	19.2	3.7
	4	1	PZE_101195591	244158 - 244596	155.9	11.2	2.5
	5	2	PZE_102161485	206123 - 207224	123	13.3	2.8
	6	3	PZE_103098655	158895 - 161562	65.7	12.7	2.7
	7	3	PZE_103128597	185274 - 187610	93.2	9.1	2.2
	8	4	PZE_104025181	29345 - 30933	51.8	22.8	4.2
	9	5	PZE_105050638	42662 - 51518	61.2	16.8	3.3
	10	6	PZE_106097991	151792	77.3	11.7	2.6
	11	7	PZE_107072354	128648 - 128709	68.9	14.8	3.1
	12	8	PZE_108061059	107884 - 109378	60.7	27.9	5
	13	9	PZE_109010476	11398	30.3	11.4	2.5
	14	9	PZE_109094832	141175	82.6	5.1	1.6
	15	10	PZE_110047800	89438 - 106051	47.4	93	15.2
DtTAS(d)	1	1	PZE_101033489	21569 - 22464	43	12.1	2.5
	2	1	PZE_101140981	182104 - 184245	105	41.4	6.6
	3	1	PZE_101216412	267537 - 267568	171.5	12.3	2.5
	4	3	PZE_103098655	158895 - 161562	65.7	30.9	5.1
	5	3	PZE_103152007	205694	109.8	11.3	2.4
	6	4	PZE_104022348	23525 - 25988	49.6	25.7	4.4
	7	5	PZE_105059330	58137 - 72409	66	29.1	4.9
	8	5	PZE_105138874	193728	108.2	7.8	1.9
	9	6	PZE_106090469	147428	71.3	6.8	1.7
	10	7	PZE_107040665	66316 – 171898	75.4	13.6	2.7
	11	7	PZE_107130789	171926	126.3	6.2	1.6
	12	8	PZE_108018453	18973	42.2	11.8	2.4
	13	8	PZE_108070788	123843	69.2	20.3	3.6
	14	9	PZE_109020361	20598 - 20829	47.7	10.7	2.3
	15	9	PZE_109089874	137784	78	10.3	2.2
	16	9	PZE_109119196	153947	120.8	6.8	1.7
	17	10	PZE_110050293	94969 - 106961	47.5	77	12
PH (cm)	1	1	PZE_101021455	12363	29.3	5.1	1.4
	2	1	PZE_101106839	111278 - 150672	93.9	20.8	3.7
	3	1	PZE_101184213	229073	145.9	13.7	2.7
	4	2	PZE_102011812	5379	17.1	5.9	1.6
	5	2	PZE_102076989	59015 - 62213	74.2	20.2	3.6
	6	2	PZE_102169349	212884	128.1	9.6	2.1
	7	3	PZE_103017768	10455	33.7	8.1	1.9
	8	3	PZE_103132826	188571 - 188925	94.8	11.8	2.5
	9	3	PZE_103175533	221582 - 221583	135.2	7.1	1.8
	10	4	PZE_104022152	23948 - 24979	49.7	13.8	2.7
	11	4	PZE_104132688	215436 - 227111	120.7	9	2

12	5	PZE_105084182	101590 - 150275	73.1	9.6	2.1
13	5	PZE_105152260	203315	120.3	7.4	1.8
14	6	PZE_106049618	98629	30.4	21.2	3.8
15	7	PZE_107072030	128141 - 128146	66.4	18	3.3
16	7	PZE_107126258	168905	115.7	10.4	2.3
17	8	PZE_108009237	9875	25.6	7.3	1.8
18	8	PZE_108056704	101776 - 102656	57	8.1	1.9
19	8	PZE_108096469	152593 - 153140	85.5	17.3	3.2
20	9	PZE_109077113	124694 - 130885	70.9	19.7	3.6
21	10	PZE_110047799	89438 - 97551	46.6	77.4	12.2